Interdependence of Nucleation, Elongation, and Bundling in the Assembly of Crosslinked Actin Structures

A THESIS SUBMITTED TO THE FACULTY OF THE UNIVERSITY OF MINNESOTA

BY

Laura A. Sherer

IN PARTIAL FULFILLMENT OF THE REQUIREMENTS FOR THE DEGREE OF DOCTOR OF PHILOSOPHY

Advisor: Dr. Naomi Courtemanche

July 2022

ACKNOWLEDGEMENTS

I would first like to thank my advisor, Dr. Naomi Courtemanche, for being an outstanding mentor. She provided the perfect amount of encouragement and challenge, and I very much appreciate all the time and effort she has invested in my scientific development. I'm grateful for the opportunity to learn from such a rigorous and talented scientist.

I also want to thank my lab mates Mark Zweifel and Biswaprakash Mahanta for their support and for putting up with my aggressively loud typing. Mark was very patient and a great resource for advice. Biswa was always helpful and has become a dear, lifelong friend.

I also want to acknowledge my committee, Dr. Melissa Gardner, Dr. Mary Porter, Dr. Nicholas Levinson, and Dr. Sivaraj Sivaramakrishnan for their excellent guidance. I'd like to thank the Titus, Clarke, and Gardner labs for their feedback during group lab meetings. Dr. Melissa Gardner and Dr. Margaret Titus deserve a special shoutout because they gave me so many valuable comments over the years. I benefitted greatly from their mentorship.

I'd like to acknowledge the UMN graduate student community for their comradery, which buoyed me through the ups and downs of this project. I'm also very grateful for my family and their consistent support; I would not have reached this stage of my education without them. I thank my grandpa and dad for teaching me the joy of learning and curiosity, and I thank my mom and dad for their incredible selflessness. Lastly, I'd like to acknowledge my partner, Soumya Mukherjee, for always having time for a good conversation.

ABSTRACT

Remodeling of the actin cytoskeleton drives essential cell processes like morphogenesis, motility, and cytokinesis. A network of actin-binding proteins tightly regulates each stage of actin dynamics, leading to the coordinated assembly of higher-order actin structures that are specialized for specific cellular roles. Many of these cytoskeletal assemblies are made from unbranched actin filaments that are crosslinked into actin bundles or meshworks. Cells generate unbranched filaments using proteins called formins, which control both actin filament nucleation and elongation. After filaments are formed, they are held together in specific geometries by crosslinkers like fascin. Within the dynamic cellular environment, the processes of nucleation, elongation, and crosslinking take place concurrently. Thus, to understand the assembly of actin structures, we need to know how these processes are integrated together. To investigate this interdependence, I developed TIRF microscopy-based assays and computational image analysis pipelines to visualize, quantify, and characterize reconstituted actin filaments and crosslinked actin structures. I first employed these tools to dissect the contributions of formin-mediated nucleation and elongation to actin filament assembly, finding that the dependence of filament length on the elongation rate is limited by formin's nucleation activity. I next explored how elongation influences fascin-mediated bundling during the assembly of crosslinked actin structures. I found that bundling of filaments earlier in elongation prevents discrete bundles from merging together to form interconnected meshworks. These results indicate that uncoordinated filament elongation and crosslinking can alter the architecture of bundled actin networks. Taken together, these studies offer important insight into the integration of nucleation, elongation, and crosslinking and provide a framework for future investigations into the assembly of specialized actin structures.

TABLE OF CONTENTS

LIST OF TABLES

LIST OF FIGURES

DISCLAIMER

Parts of this thesis have been directly adopted or paraphrased from the published literature of my work (Sherer et al., 2018; Zweifel et al., 2021; Sherer and Courtemanche, 2022).

CHAPTER 1. Introduction

The Importance of Actin Dynamics to Cell and Tissue Function

Actin is one of the most abundant and highly conserved proteins in eukaryotes (Dominguez and Holmes, 2011). It assembles into filamentous scaffolds that drive key cellular functions during development and homeostasis. Discovered in the 1940s in skeletal muscle (Bugyi and Kellermayer, 2020), actin first gained prominence as a component of the sarcomere, which is the highly-ordered and stable structure upon which muscle contraction depends. Yet, even then, researchers recognized actin's ability to switch from globular to filamentous forms (Bugyi and Kellermayer, 2020). Today, actin's dynamic nature is known to be a critical aspect of its biological and cellular function. For example, a cell undergoing cytokinesis typically builds, remodels, and disassembles an actomyosin contractile ring in < 1 hour (Pollard and Wu, 2010; Kothari et al., 2017), and cell motility is driven by polarized actin polymerization and coordinated changes to actin-dependent adhesion (Rørth, 2009). In addition to division and motility, actin remodeling mediates endocytosis, mechanotransduction, and synapse formation (Gordon-Alonso et al., 2010; Mooren et al., 2012; Lei et al., 2016; Harris et al., 2018). Actin-supported cell behaviors also lead to the emergence of more complex phenotypes at the tissue and organismal levels, like wound healing, the immune response, and tissue morphogenesis.

Numerous diseases are linked to the dysregulation of actin cytoskeletal dynamics. For example, mutations in actin regulating proteins underlie blood disorders like macrothrombocytopenia, primary immunodeficiencies, the kidney disease focal segmental glomerulosclerosis, and neurological pathologies such as amyotrophic lateral sclerosis (ALS)(Feng et al., 2015; Kallikourdis et al., 2015; Murphy et al., 2016; Labat-de-Hoz and Alonso, 2021; Murk et al., 2021). Moreover, intracellular pathogens like

Listeria monocytogenes co-opt their host's actin cytoskeleton and use the stolen molecular machinery to propel themselves through the cytosol and wreak havoc (Lambrechts et al., 2008). Cancer cells also use actin structures to facilitate the migratory and invasive behaviors that contribute to cancer progression and metastasis, which is the most common cause of mortality in cancer patients (Alizadeh et al., 2014).

Actin Filaments and Higher-Order Actin Structures

Although there are cellular roles for monomeric actin (Kapoor et al., 2013), the functional importance of actin largely comes from the ability of monomers to noncovalently polymerize into filaments. During polymerization, actin monomers undergo a structural transition where its two major lobes twist with respect to each other, moving from a skewed conformation to the flattened one observed in actin filaments (Dominguez and Holmes, 2011). Due to the structural asymmetry of actin monomers, actin filaments are polar, and filament ends (called the barbed and pointed end) exhibit dramatically different polymerization properties (see *Overview of Actin Filament Nucleation and Elongation*). In addition, actin filaments are also helical and can be described as a single, left-handed helix or a double, right-handed helix (Jegou and Romet-Lemonne, 2020).

During polymerization, filaments are assembled into higher-order actin structures that are specialized for distinct functions (Figure 1). For example, endocytic actin patches are composed of branched actin filaments that are very short (< 200 nm) and highly crosslinked (Young et al., 2004; Sirotkin et al., 2010). This arrangement results in geometric constraints that converts crosslinker binding energy into elastic energy that can later be turned into mechanical work for membrane invagination (Ma and Berro, 2018). On the other hand, cytokinetic rings consist of bundles of unbranched filaments

that are oriented in different directions (“antiparallel”). This mixed polarity allows myosin to pull the bundled filaments together and contract the ring during cell division (Blanchoin et al., 2014). Environment-sensing protrusions known as filopodia are also composed of bundles of unbranched actin filaments, but in this case, the filaments are all oriented in the same direction (“parallel”), with their barbed ends toward the membrane (Mattila and Lappalainen, 2008). As a result, these bundles elongate outward from the cell body. The collective push of multiple bundled filaments generates enough force to deform the membrane, thus forming a protrusive structure that can probe the cell’s environment.

Assembly of these actin structures and others like them is spatially and temporally regulated by the cell. Tight control over actin dynamics is achieved primarily by an extensive network of actin-binding proteins, which mediate actin processes like severing, nucleation, elongation, branching, and crosslinking (Pollard, 2016). In addition, many actin-binding proteins synergize and compete amongst each other, which can influence a structure’s morphology and dynamics. In the following sections, I describe some key actin processes and the actin-binding proteins that regulate them.

Overview of Actin Nucleation and Elongation

The initial steps of actin polymerization involve the self-association of monomers to form dimers and trimers called actin nuclei (Cooper et al., 1983; Sept and McCammon, 2001). Actin nuclei formation is the rate-limiting step of filament assembly due to the instability of nuclei compared to filaments (Sept and McCammon, 2001). Yet, although nucleation is energetically unfavorable, physiological actin concentrations (50-250 μM in non-muscle cells) are high enough to permit spontaneous nucleation. As a result, cells employ actin monomer-binding proteins to prevent unrestrained filament assembly. One notable example of such a protein is profilin, a structurally conserved actin regulator that

binds to the barbed end groove and hinders aberrant nucleation (Courtemanche and Pollard, 2013; Murk et al., 2021).

To assemble filaments in a controlled manner, cells must overcome inhibition of nucleation by profilin using actin-binding proteins that enhance nucleation. For example, the Arp2/3 complex nucleates new branches off the sides of filaments, thus generating networks of branched actin. Other proteins like Spire and Cordon-bleu (Cobl) promote nucleation of unbranched filaments by binding to multiple monomers simultaneously, thus clustering them and increasing the probability of nuclei formation (Quinlan et al., 2005; Ahuja et al., 2007). However, the most prominent nucleators of unbranched actin filaments are formins (see *Formin-Mediated Actin Nucleation and Elongation*).

Following nucleation, actin filaments elongate through the addition of monomers to either filament end. Due to the polarity of actin filaments, the rates of barbed end elongation (k_{on} = ~10 μM^{-1} s^{-1}) are significantly faster than the pointed end (k_{on} = ~1 μM^{-1} s^{-1})(Kuhn and Pollard, 2005). This difference is exaggerated by actin polymerases like Ena/VASP and formins, which associate with the barbed end and further speed up elongation (Romero et al., 2004; Winkelman et al., 2014).

Formin-Mediated Actin Nucleation and Elongation

Cells assemble unbranched filaments using a family of actin-binding proteins called formins (Chang et al., 1997; Schirenbeck et al., 2005; Lizárraga et al., 2009; Mellor, 2010; Jaiswal et al., 2013)(Table 1). These important actin regulators are characterized by a ~400 amino acid long, highly conserved domain known as the formin homology 2 (FH2) domain (Higgs, 2005; Higgs and Peterson, 2005). Formins are found in the overwhelming majority of eukaryotes studied, but the number of formin isoforms varies significantly across species (Chalkia et al., 2008). Mammals express 15 different

isoforms, which makes it difficult to comprehensively study formins in mammalian systems (Higgs, 2005). However, budding and fission yeast only express 2 and 3 formins, respectively, and loss of any one isoform results in disrupted actin dynamics and functional defects, which suggests that formins play non-redundant biological roles in cells (Chang et al., 1997; Petersen et al., 1998; Ozaki-Kuroda et al., 2001; Pruyne et al., 2004; Buttery et al., 2007).

Although some isoforms exhibit specialized activities, formins are best known as regulators of actin nucleation and elongation (Figure 2). Typically located on the C-terminal end of the protein, formin FH2 domains homodimerize in a head-to-tail manner and form a ring-shaped structure that encircles actin nuclei (Pring et al., 2003; Xu et al., 2004; Otomo et al., 2005; Lu et al., 2007; Thompson et al., 2013). This interaction prevents the dissociation of monomers from nuclei, thereby promoting new filament formation. The efficiency of formin-mediated nucleation varies across different isoforms. For example, the budding yeast formin Bnr1 nucleates actin with >10-fold greater efficiency compared to the other budding yeast formin, Bni1 (Moseley and Goode, 2005).

In addition to actin nuclei, FH2 domains also encircle filament barbed ends and remain processively attached as new actin subunits are added to the filament (Pruyne et al., 2002; Zigmond et al., 2003; Mizuno et al., 2011; Breitsprecher et al., 2012). The presence of the FH2 domain on filament barbed ends affects the favorability of new monomer addition, leading to altered rates of elongation (Aydin et al., 2018). Molecular dynamics simulations suggest this effect arises from steric interference and conformational distortion of the terminal actin subunits. In this way, the FH2 domain slows filament elongation compared to spontaneous actin polymerization. However, the extent of this slowdown is highly variable across different formin isoforms. For example, FH2 dimers from mammalian Diaphanous-1 (mDia1) reduce filament elongation rates by

only ~5% (Kovar et al., 2006). At the other extreme, the FH2 domains of Cdc12p from fission yeast and delphilin from mammals both reduce elongation rates by >99% (Kovar et al., 2003; Dutta et al., 2017; Silkworth et al., 2018).

The direct binding of actin monomers to formin-bound filament ends is known as the FH2 pathway of formin-mediated elongation. However, formins can also incorporate new subunits into filaments by using their formin homology 1 (FH1) domain, which cooperates with the monomer-binding protein profilin (Courtemanche, 2018). Typically N-terminal adjacent to the FH2 domain, FH1 domains consist of rigid proline-rich tracts that are interspersed with flexible regions of intrinsically disordered “spacer” sequences. Profilin can bind to the proline-rich tracts through its Src Homology 3 (SH3) motif, and it has a greater affinity for these tracts when bound to an actin monomer. After binding to a polyproline tract, the profilin-actin complex is then delivered to the barbed end of the filament by the FH1 (Figure 2). This delivery is a diffusion-mediated process that is facilitated by the flexibility of the intrinsically disordered spacers (Horan et al., 2018). By funneling actin monomers to the barbed end, the FH1 domain significantly enhances rates of filament elongation and overcomes FH2-mediated slowdowns.

Elongation rate enhancements by the FH1 vary considerably across formin isoforms, likely due to differences in the numbers and lengths of polyproline tracts (Higgs, 2005). In particular, the number of tracts seem to positively correlate with rates of formin-mediated elongation. For example, mDia1 has 14 polyproline tracts and elongates filaments very quickly (47 subunits/s), whereas Cdc12p has only two tracts and elongates filaments slowly (12-13 subunits/s) (Kovar, 2006).

The diversity of formins’ actin assembly properties and the prevalence of these proteins across different cellular processes suggest that formins may be important for finetuning of actin filament dynamics in cells.

Actin Filament Crosslinking

As they elongate, actin filaments are assembled into an array of higher-order actin structures. Crosslinking is a critical aspect of this assembly because it mechanically couples individual actin filaments, which otherwise bend at physiologically-relevant lengths (> 10 μm, the persistence length of actin) (Isambert et al., 1995; McCullough et al., 2008). Even short actin filaments (< 5 μm) can buckle under cellular forces caused by confinement or myosin motor protein activity (Kovar and Pollard, 2004; Blanchoin et al., 2014). Moreover, a polymerizing single filament only generates a few piconewtons of outward force, which is not enough to deform the membrane (Blanchoin et al., 2014). As a result, the mechanical reinforcement conferred by crosslinking make it vital for proper actin structure assembly and overall cellular function.

Crosslinked actin structures have diverse geometries that make them well-suited for specific cell processes. In filopodia and contractile rings, actin filaments are bundled in parallel or antiparallel orientations (Mattila and Lappalainen, 2008; Courson and Rock, 2010; Laporte et al., 2012). In the actin cortex, filaments are unaligned and crosslinked into meshworks (Chugh et al., 2017; Svitkina, 2020). To facilitate assembly of these different arrangements, cells express a variety of crosslinker proteins that impart structures with distinct physical attributes. For example, alpha-actinin is a relatively flexible crosslinker that generates bundles of mixed polarity with wide inter-filament spaces (~35 nm) (Hampton et al., 2007; Courson and Rock, 2010). This geometry is compatible with myosin-mediated contractility, and as a result, alpha-actinin localizes to contractile structures like the cytokinetic ring and stress fibers (Blanchoin et al., 2014). Filamin A is also a flexible crosslinker, but it connects perpendicularly oriented filaments, which helps generate the actin meshwork at the cortex (Flanagan et al., 2001). This

cortical architecture is required for proper cell locomotion and other dynamic cell shape changes (Flanagan et al., 2001; Chugh et al., 2017).

The Bundling Protein Fascin

Amongst the many crosslinkers in the cell, the bundling protein fascin is of particular interest due its distinct bundle phenotype and physiological importance. In humans, there are three fascin isoforms. Expression of fascin-2 and fascin-3 are limited to the retina, inner hair cells, and testis (Hashimoto et al., 2011; Perrin et al., 2013). In contrast, fascin-1 (hereafter referred to as fascin) is more widely expressed, especially during development (Lamb and Tootle, 2020). In healthy adults, fascin is found in neuronal cells, dendritic cells (a type of innate immune cell), and vascular endothelial cells (Zhang et al., 2008).

On the molecular level, fascin is a monomeric bundler composed of four beta-trefoil domains that come together to create 2 (perhaps 3) different actin filament binding sites (Jansen et al., 2011; Yang et al., 2013). Unlike alpha-actinin or Filamin A, fascin forms bundles of parallel filaments, which is the simplest arrangement for a crosslinked actin structure. Also, the stiff and compact nature of a fascin monomer leads to very rigid fascin-assembled bundles with narrow inter-filament spaces (~8 nm) (Claessens et al., 2006).

These molecular characteristics make fascin well-suited for its stabilizing role in polarized protrusions like filopodia, invadopodia, and dendritic cell membrane extensions (Vignjevic et al., 2006; Li et al., 2010; Yamakita et al., 2011; Van Audenhove et al., 2016). Filopodia are thin protrusive structures that help a cell sense its environment during processes like neuronal pathfinding, angiogenesis, and cancer metastasis (Mattila and Lappalainen, 2008; Arjonen et al., 2011). Depletion of fascin leads to fewer

and shorter filopodia that exhibit a “wavy” morphology, which suggests that the bundling protein enhances filopodia stiffness (Vignjevic et al., 2006; Van Audenhove et al., 2016). In addition, fascin also localizes to invadopodia, which are structures that mediate extracellular matrix adhesion and degradation in cancer cells (Li et al., 2010; Van Audenhove et al., 2016). These ventral protrusions have a branched actin base with an elongated tip comprised of fascin-rich bundles of unbranched filaments (Li et al., 2010; Murphy and Courtneidge, 2011; Van Audenhove et al., 2015). Knockdown of fascin in the human melanoma cell line CHL-1 decreases the number, length, and lifetime of invadopodia and reduces their matrix degradation activity (Li et al., 2010; Van Audenhove et al., 2014, 2016). As a result of these changes, fascin-depleted cells also exhibit reduced invasive migration into 3D collagen gels. Strikingly, the correlation between fascin downregulation and diminished cell migration or invasion has been replicated in over 30 different cell lines (Liu et al., 2021). The converse relationship for fascin upregulation is also very robust (>20 different cell lines).

Fascin’s association with migratory and invasive cell behaviors suggests that it may be a driver of cancer metastasis in humans. Indeed, tumors with higher fascin expression levels are more likely to metastasize, and high fascin cohorts also tend to have a poorer prognosis and reduced survival times (Tan et al., 2013; Liu et al., 2021). This relationship and fascin’s low expression in healthy adult epithelium have led to its emergence as a possible biomarker or therapeutic target.

State of the Field and Open Questions

Cells assemble crosslinked actin structures with distinct morphological and dynamic properties that allow them to carry out specific processes like cytokinesis and motility. Many of the major molecular players that regulate actin structure assembly are well-

established. These players include formins and fascin, whose nucleation, elongation, and crosslinking activities have been characterized previously.

Construction of crosslinked actin structures in cells frequently involves the co-occurrence of multiple actin processes (Figure 3); for example, actin filaments in cytokinetic rings and filopodia undergo elongation and crosslinking at the same time (Mallavarapu and Mitchison, 1999; Tang et al., 2015). Yet, most of the research on actin dynamics has focused on studying individual reactions. To understand how cells assemble complex actin structures, we need to build upon this pioneering foundational knowledge and examine the interdependence of different actin processes.

This is not an easy task. In both cells and *in vitro* systems, it is difficult to uncouple two interrelated, highly dynamic reactions while still preserving their original relationship. Observations in cells are particularly difficult to interpret because of the extreme overcrowding in the cellular environment. Even in simpler systems, useful insights on actin dynamics can be overlooked due to the information-dense nature of microscopy data and the inefficiency of manual image analysis. Because of these challenges, there are still many open questions about how different actin processes interact with each other.

For example, formins utilize a common pool of monomers to both nucleate and elongate actin filaments. Cellular activation of formins triggers both activities. It is not clear how different formins balance their nucleation and elongation reactions to assemble the correct number of filaments that are the appropriate length for a functional actin structure. Does the elongation rate dominate the reaction and dictate filament numbers and lengths, or does the nucleation efficiency matter more? Understanding this balance may provide insight into the underlying logic that connects the properties of formin isoforms with the specific structures they build.

Interactions between elongation and crosslinking also requires more investigation. Although straightforward at the individual filament level, recent evidence suggests that this relationship becomes more complex in filament populations. For example, researchers found that rates of actin polymerization determine the architecture of crosslinked actin structures assembled *in vitro* by the crosslinker alpha-actinin, shifting them from a population of sparse, thick bundles to a dense meshwork (Falzone et al., 2012, 2013). Though these excellent studies establish a link between actin polymerization and crosslinked structure morphology, many questions remain. For example, alpha-actinin is a flexible, promiscuous crosslinker (Courson and Rock, 2010), but does a stiff crosslinker like fascin produce the same effect? Also, the experimental conditions used in these initial studies result in changes to both nucleation (i.e., the number of filaments) and elongation, so it is still unclear how the assembly of crosslinked structures evolves as a set number of filaments elongate. It is also unknown whether the length at which filaments initially become crosslinked influences the overall morphology of the resultant actin network.

In this thesis, I address some these knowledge gaps. In Chapter 2, I discuss a method to reconstitute distinct actin filament populations and image them using total internal reflection fluorescence (TIRF) microscopy. I also describe assays that enable real-time visualization of actin filament bundling in a way that captures both individual crosslinking events and the broader morphological and dynamic properties of crosslinked actin structures. In Chapter 3, I describe custom-built MATLAB programs used to analyze the wealth of imaging data generated by the experiments outlined in Chapter 2. First, I discuss a computational tool that quickly quantifies the numbers and lengths of actin filaments in TIRF micrographs, which act as readouts for nucleation and elongation, respectively. Secondly, I describe a program that automates bundle

detection from TIRF microscopy movies, which greatly facilitates kinetic analysis of bundling.

In Chapter 4, I dissect the contributions of nucleation and elongation to actin filament assembly for different formin isoforms, finding that the dependence of filament length on the elongation rate is limited by formin's nucleation activity. In Chapter 5, I explore how elongation influences fascin-mediated bundling during the assembly of crosslinked actin structures. The data reveal that bundling of filaments earlier in elongation establishes a template that constrains bundle flexibility, which prevents bundles from coalescing into interconnected meshworks. These results suggest that uncoordinated filament elongation and crosslinking can alter the morphology of actin bundled networks.

Taken together, this work provides meaningful insight into how actin filament nucleation, elongation, and crosslinking are integrated to form specific types of complex actin structures capable of driving essential cell functions.

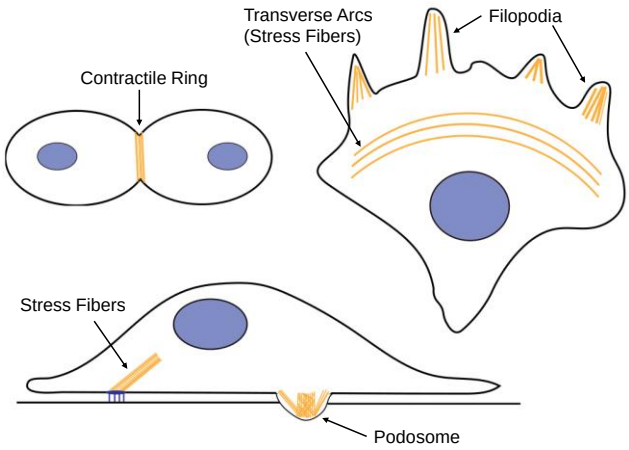

Figure 1. Examples of crosslinked actin structures. Individual actin filaments are assembled into diverse higher-order actin structures that drive essential processes like motility, division, and adhesion.

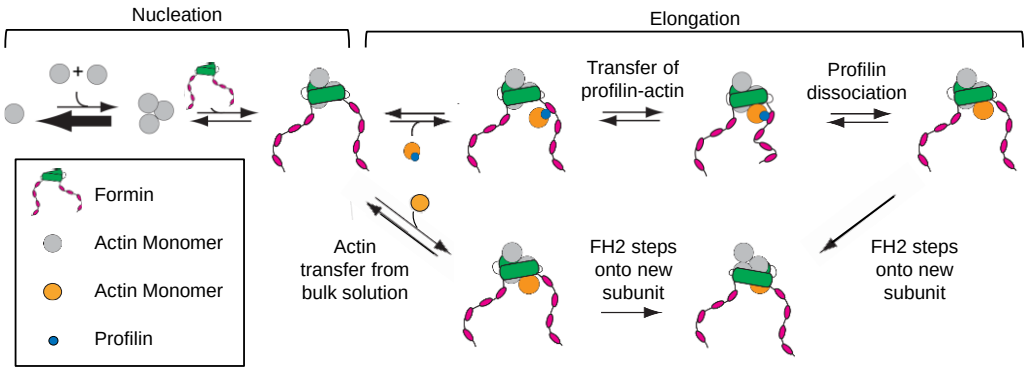

Figure 2. Formin-mediated actin filament assembly. Formins stabilize actin nuclei and also bind to the fast-growing barbed end of actin filaments, where they affect elongation through two major pathways. One pathway is profilin-independent and involves the direct binding of actin monomers to FH2-bound filament ends. The other pathway involves profilin-actin binding to polyproline tracts on the FH1 domain (pink circles), which then delivers the profilin-actin to the filament end. Formins remain processively attached to barbed ends, so in both pathways, the last step is the FH2 stepping onto the new subunits to begin the cycle again.

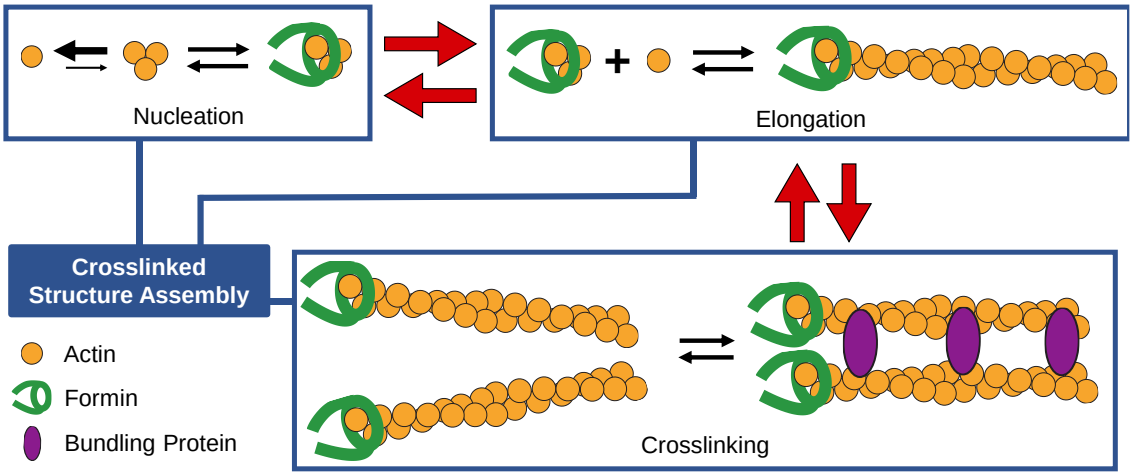

Figure 3. Model for the assembly of crosslinked actin structures. Actin filament nucleation, elongation, and crosslinking occur concurrently during the assembly of higher-order actin structures. The goal of this thesis is to understand the interactions between these dynamic actin processes during crosslinked structure assembly.

Actin Structure	**Formin** (Organism)	**Crosslinker**	**Function**
Invadopodia/ Podosomes	**FMNL1** (Mammals) (Mersich et al., 2010), **FHOD1** (Mammals) (Panzer et al., 2016) **INF2** (Mammals) (Panzer et al., 2016)	**Fascin** (Li et al., 2010; Van Audenhove et al., 2015) **Alpha-Actinin** (Yamaguchi et al., 2017)	**Substrate Adhesion, ECM Degradation**
Stress Fibers	**mDia1** (Mammals) (Valencia et al., 2021) **mDia2** (Mammals) (Gupton et al., 2007) **FHOD1** (Mammals) (Schulze et al., 2014)	**Alpha-Actinin** (Kovac et al., 2013)	**Cell Contraction, Substrate Adhesion, Mechano-transduction**
Cytokinetic Rings	**mDia2** (Mammals) (Watanabe et al., 2013) **Cdc12** (Mammals) (Chang et al., 1997)	**Alpha-Actinin** (Fujiwara et al., 1978)	**Cell Division**
Filopodia	**mDia1** (Mammals) (Goh et al., 2011) **mDia2** (Mammals) (Yang et al., 2007) **DAAM1** (Mammals) (Jaiswal et al., 2013) **FMNL2** (Mammals) (Pfisterer et al., 2020)	**Fascin** (Vignjevic et al., 2006) **Fimbrin / L-plastin** (Van Audenhove et al., 2016)	**Environment-Sensing**
Actin Cortex	**mDia1** (Mammals) (Chugh and Paluch, 2018)	**Alpha-Actinin** (Mukhina et al., 2007), **Filamin** (Razinia et al., 2012)	**Cell Mechanics and Cell Shape Changes**
Actin Cables	**Bni1** (*S. cerevisiae*) (Buttery et al., 2007) **Bnr1** (*S. cerevisiae*) (Buttery et al., 2007) **For3** (*S. pombe*) (Feierbach and Chang, 2001)	**Fimbrin** (Skau et al., 2011)	**Cargo Transport**
Cardiac Sarcomere	**FHOD3** (Mammals) (Martin and Kirk, 2020)	**Alpha-Actinin** (Martin and Kirk, 2020)	**Heart Muscle Contraction**

Table 1. Formins and crosslinkers in diverse actin structures.

CHAPTER 2. Experimental Methods

Actin Purification

Actin was extracted from chicken skeletal muscle and purified by one cycle of polymerization and depolymerization (Spudich and Watt, 1971). Monomers were separated from oligomers and filaments via gel filtration with a Sephacryl S-300 resin (GE Healthcare) in G-buffer (2 mM Tris, pH 8.0, 0.2 mM ATP, 0.5 mM DTT, 0.1 mM $CaCl_2$). Fluorescent actin for experiments with elongating bundles was generated by labeling Cysteine 374 with Oregon Green 488 iodoacetamide (Kuhn and Pollard, 2005).

Formin Purification

Constructs encoding the FH1 and FH2 domains of the formin Cdc12p (residues 882-1375) and Bni1p (1329-1375) were cloned into pGEX-4T-3 (GE Healthcare) vectors with an N-terminal glutathione *S*-transferase (GST) tag adjacent to a Tobacco Etch Virus (TEV) protease recognition sequence and a C-terminal polyhistidine tag.

Formins were expressed in BL21(DE3) RP Codon Plus cells (Agilent) in 1 L of LB, induced with 0.5 mM IPTG at OD_{600} ~0.6, and incubated overnight at 17°C. Harvested cells were sonicated in lysis buffer (50 mM Tris, pH 7.5, 500 mM NaCl, 1 mM DTT, and 10% glycerol) and centrifuged at 4°C for 40 minutes at 31,000 x *g*. Cell lysates were incubated with glutathione agarose resin for 1 hour with rotation at 4°C. Samples were washed with lysis buffer and low salt wash buffer (50 mM Tris, pH 7.5, 100 mM NaCl, 1 mM DTT, 10% glycerol). Formins were eluted with 6 mL of elution buffer (50 mM Tris,100 mM NaCl, 100 mM glutathione, pH 7.5, 10% glycerol). To remove the GST-tag, the eluted fraction was incubated with TEV protease overnight at 4°C. Remaining contaminants (like cleaved GST tags and TEV proteases) were eliminated using nickel affinity chromatography. Samples were washed (50 mM Tris, pH 7.5, 300 mM NaCl,

10% glycerol) on the column and eluted with 6 mL of elution buffer (50 mM Tris, pH 7.5, 300 mM NaCl, 10% glycerol, 250 mM imidazole). Purified protein was concentrated via centrifugal filters (MilliporeSigma Amicon, MWCO 30K) and dialyzed into storage buffer overnight at 4˚C (50 mM KCl, 1 mM MgCl2, 1 mM EGTA, 10 mM imidazole, 10% glycerol). Samples were flash frozen and stored at -80°C.

Fascin Purification

Human fascin-1 was expressed in BL21(DE3)pLysS cells from a pET21a plasmid that was modified to encode an N-terminal GST tag and Tobacco Etch Virus (TEV) protease cleavage recognition sequence. Transformants were grown in 1 L of LB broth, induced at OD_{600} ~0.6 with 0.5 mM IPTG, and shaken at 16 °C overnight. To purify fascin, resuspended cell pellets were sonicated in lysis buffer (50 mM Tris, pH 8.0, 500 mM NaCl, 1 mM DTT) and centrifuged (~31,000 x *g*, 4°C) for 40 minutes to isolate soluble cell components. Lysates were incubated with glutathione agarose resin (pH 8.0) for one hour with rotation at 4°C, washed with low-salt buffer (50 mM Tris, pH 8.0, 100 mM NaCl, 1 mM DTT), and eluted (50 mM Tris, pH 8.0, 100 mM NaCl, 1mM DTT, 100 mM glutathione). The eluted protein was incubated with maltose-binding protein (MBP)-tagged TEV protease at 4 ºC overnight to remove the GST tag. Samples were dialyzed into low-salt buffer, followed by a 1-hour incubation with glutathione agarose resin to remove the cleaved GST tag. After collecting the flowthrough, TEV protease was removed by applying the sample to an amylose column and collecting the flowthrough. Pure protein samples were concentrated via centrifugal filtration (MilliporeSigma Amicon, MWCO 30K), flash-frozen, and stored at -80°C. The extinction coefficient used to calculate fascin concentration was 68,465 $M^{-1}\,cm^{-1}$.

Co-sedimentation Assays

Ca^{2+}-actin monomers were converted to Mg^{2+}-actin via the addition of 0.05 mM $MgCl_2$ and 0.2 mM EGTA. Samples containing 15 µM Mg^{2+}-actin monomers were polymerized in KMEI buffer (50 mM KCl, 1 mM $MgCl_2$, 1 mM EGTA, 10 mM Imidazole pH 7.0) for 45 minutes in the presence or absence of 250 nM Cdc12p FH1FH2 to generate short and long filaments, respectively. Polymerized samples were diluted to 2-3 µM actin and incubated with a range of fascin concentrations for 1 hour at 25˚C (Figure 4). Samples were centrifuged for 30 minutes at 10,000 x *g* (long filaments) or 20,000 x *g* (short filaments). Supernatants and pellets were separated and analyzed via SDS-PAGE. Gel band densities were quantified using Fiji and normalized by molecular weight. Fascin density on pelleted actin bundles was plotted as a function of the fascin concentration and fit with the McGhee-von Hippel equation (McGhee and von Hippel, 1974; De La Cruz, 2005) to obtain dissociation and cooperativity constants for at least three independent replicates.

Co-sedimentation assays with phalloidin-stabilized or Cdc12p-bound long actin filaments were performed as described above, except that filaments polymerized in reactions containing 15 µM Mg^{2+}-actin monomers were diluted to 2 µM actin and incubated with either 2 µM FITC-phalloidin or 100 nM Cdc12p for 20 minutes at 22 ºC prior to the introduction of fascin.

In Vitro Actin Polymerization Reactions and Visualization by TIRF Microscopy

Ca^{2+}-ATP-actin monomers were incubated with 0.05 mM $MgCl_2$ and 0.2 mM EGTA for 3 minutes to generate Mg^{2+}-ATP-actin. Actin monomers (2 µM unless otherwise stated) were polymerized in the presence and absence of Cdc12p and Bni1p in KMEI buffer (50 mM KCl, 1 mM EGTA, 10 mM Imidazole, pH 7.0) for 1 hour.

Assembled actin filaments were stabilized and fluorescently labeled via the addition of 4 µM fluorescein-isothiocyanate (FITC) phalloidin (Sigma-Aldrich, St. Louis, MO). After a 10-min incubation, samples were diluted to a final concentration of 2–10 nM actin in 2x microscopy buffer (1x microscopy buffer: 10 mM imidazole (pH 7.0), 50 mM KCl, 1 mM MgCl2, 1 mM EGTA, 50 mM DTT, 0.2 mM ATP, 15 mM glucose, 20 mg/mL catalase, 100 mg/mL glucose oxidase, 0.5% (w/v) methylcellulose (4000 cP at 2%)). 10–15 µL of each sample was loaded onto an imaging surface using pipette tips that were cut to reduce filament shearing. Filaments were visualized by through-objective total internal reflection fluorescence (TIRF) microscopy on an Olympus Ti83 motorized microscope equipped with a CellTIRF system using a 60x, 1.49 N.A. objective and a 488-nm laser. Images were acquired using a Hamamatsu C9100-23B ImagEM X2 EMCCD camera and CellSens Dimension software (Olympus). The number of filaments and their corresponding lengths were quantified (see Chapter 3) for three replicates at each formin concentration using at least five fields of view per replicate. Single exponential fits were applied to filament length distributions. For an exponential distribution, the fraction of filaments (f_i) with length l was determined by the relation $f_i = \lambda \exp(-\lambda l_i)$, where the mean length is $1/\lambda$ and the variance is $1/\lambda^2$.

Preparation of Coverslips

Coverslips (#1.5, Corning) were prepared by sonication in 2% Hellmanex III for 1 hour, followed by rinsing and sonication in ddH_20 for an additional hour. The imaging area was constructed by placing Scotch Tape around the perimeter of a 4.5 mm x 4.5 mm region of the coverslip. To prevent leaks, the coverslip was briefly exposed to a flame before use. The imaging surface was blocked with 10 µL of 0.5% (v/v) Tween 20 for 2 x 1 minute and 10 µL of 10% (w/v) BSA for 2 x 1 minute. High Salt TBS buffer ((600

mM NaCl, 50 mM Tris, pH 7.5) was used to prepare blocking solutions and to rinse the imaging area between each component. The surface was equilibrated with KMEI buffer (50 mM KCl, 1 mM EGTA, 10 mM Imidazole, pH 7.0) prior to sample placement.

Bundling Assays

Samples containing 2 µM Mg^{2+}-actin monomers were polymerized in KMEI buffer for 1 hour at 22 ºC in the absence or presence of 85 nM Cdc12p to generate long or short filaments. Following polymerization, actin filaments were incubated with 4 µM FITC-phalloidin for 20 minutes. Samples were serially diluted to 10 nM actin (long filaments) or 2 nM actin (short filaments) in microscopy buffer (10 mM imidazole, pH 7.0, 50 mM KCl, 1 mM $MgCl_2$, 1 mM EGTA, 50 mM DTT, 0.2 mM ATP, 15 mM glucose, 20 µg/mL catalase, 100 µg/mL glucose oxidase, 0.5% (w/v) methylcellulose (4,000 cP at 2%)). These dilutions yield identical concentrations of filaments for samples containing short and long filaments. Samples were transferred to imaging surfaces that were constructed as described above. After collecting baseline images of the samples, fascin was introduced to initiate bundling (Figure 5). Reactions were visualized at 10-30 s intervals for 20-60 minutes by TIRF microscopy as described above. Bundle assembly was analyzed as described in Chapter 3.

For assays with elongating bundles, short filaments were generated by polymerizing 2 µM Mg^{2+}-ATP-actin with 85 nM Cdc12p for 1 hour at 22 ºC and labeled with an equimolar concentration of FITC-phalloidin for 20 minutes. Samples containing 0.25 µM polymerized actin were then incubated with 1 µM fascin for 30 minutes to bundle filaments. Bundles were diluted to concentrations corresponding to 5 nM actin in microscopy buffer containing 10 µM *S. pombe* profilin, 1 µM fascin, and 0.75 or 1.5 µM Mg^{2+}-ATP-actin (5% Oregon Green-labeled). Reactions were visualized by TIRF

microscopy and performed in triplicate with up to three 80 µm x 80 µm imaging fields analyzed per replicate.

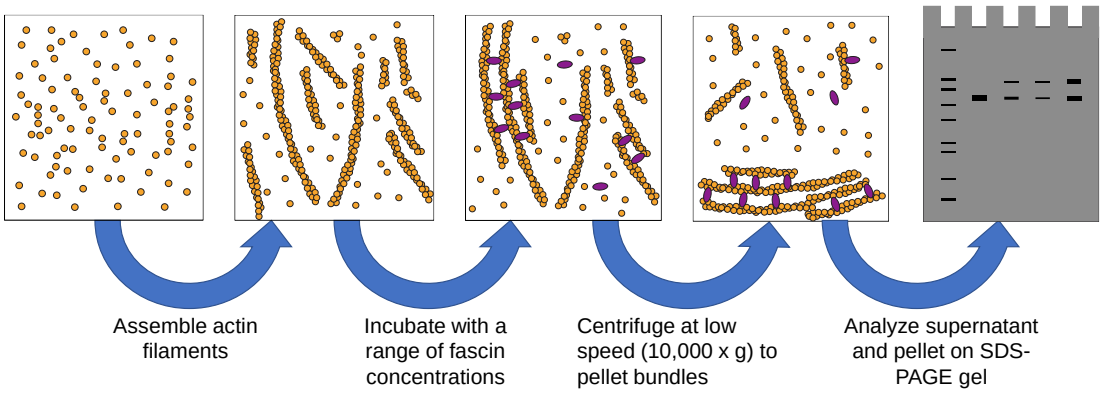

Figure 4. Low-speed co-sedimentation assays. Schematic showing the workflow for low-speed co-sedimentation assays, which measure fascin (purple ovals) binding to actin (orange circles) filament bundles.

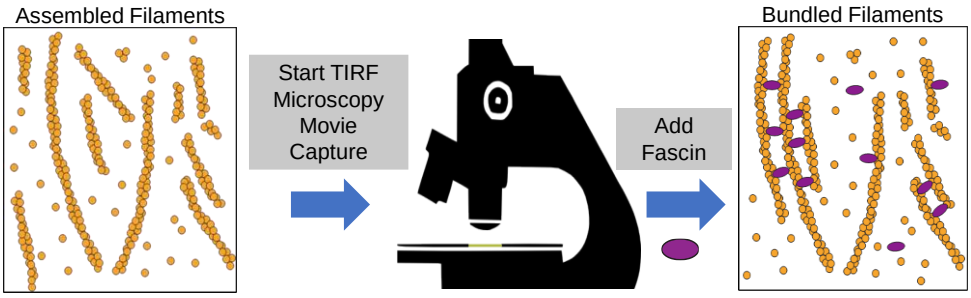

Figure 5. Bundling assays. In these experiments, actin filaments are assembled with or without formins and stabilized with fluorescent phalloidin. Baseline images of the samples are captured with TIRF microscopy. Fascin is subsequently added, and bundle assembly is visualized in real-time.

CHAPTER 3. Computational Tools to Quantify Actin Filaments and Bundles

Introduction

Automated image analysis provides many advantages over manual analysis. For example, automation improves reproducibility through the elimination of human-introduced errors and biases. It also significantly reduces the time required for analysis, which is particularly useful for large volumes of information-dense microscopy data. In some cases, this time-savings is not just convenient but also necessary to make certain types of analysis feasible. Because of these advantages, I sought out automated and semi-automated tools to assist my investigations into nucleation, elongation, and crosslinking. More specifically, I looked for tools to count the number of actin filaments present in TIRF micrographs, measure their lengths, and quantify the formation of filament bundles over time.

Typical fluorescence micrographs of polymerization reactions contain numerous actin filaments (20-200) of varying lengths. The filaments adopt random orientations on the imaging surface, resulting in frequent overlaps (Figure 6-8). In reactions with fascin, filaments are incorporated into bundles, which correlates with a dramatic increase in fluorescence intensity signal (Figure 9). Bundles often contain a mixture of crosslinked regions (i.e., consisting of multiple overlapping filaments) and single filament regions (i.e., containing no crosslinked filaments). To automate analysis of this microscopy data, I first assessed the suitability of existing computational tools like ImageJ, which is a powerful open-source software that can quantify the number of objects, object area, and other valuable metrics in a semi-automated manner (Baviskar, 2011; Grishagin, 2015). However, ImageJ is not optimized for analyzing filamentous objects that frequently overlap and vary drastically in fluorescence intensity, so it was not appropriate for the analysis of filaments or bundles.

Computational tools that were specifically designed for quantifying filamentous objects had other drawbacks. For example, one program (Falzone et al., 2012) was built for analyzing large bundles in images acquired via confocal microscopy, which has a minimum optical sectioning of ~600 nm compared to the 100 nm sections of TIRF microscopy. As a result, this group's algorithm was not designed to identify individual filaments or small bundles, so it was not well-suited for the analysis of TIRF micrographs, which advantageously provide single filament resolution.

Due to the absence of existing tools, I developed my own image analysis pipelines optimized for quantifying filaments and bundles from TIRF micrographs. The first pipeline quantifies filament lengths and numbers at a single timepoint, whereas the other measures actin bundle assembly over time.

Overview of Actin Filament and Bundle Detection

Both pipelines begin with background subtraction and noise filtering of fluorescence micrographs. To identify filaments or bundles, the programs use MATLAB's global or adaptive thresholding algorithms, which involve setting an intensity threshold to distinguish objects in the foreground from the background. Global thresholding establishes one threshold for the entire image and generally works better for micrographs containing single filaments or smaller bundles. Adaptive thresholding determines multiple thresholds based on the local context and is better suited for images containing thick bundles because of the drastic intensity differences in these micrographs. After thresholding, the programs skeletonize the detected objects using MATLAB's bwskel function, which converts rounded objects into their one pixel-wide centerlines (Figure 6). This is a key step for the accurate detection of filamentous objects like actin filaments or bundles. After skeletonization, the two pipelines diverge.

Pipeline for Quantifying Filament Numbers and Lengths

My first goal was to count the number of filaments contained in fluorescence micrographs and to quantify their lengths. These parameters provide insight into the relative efficiency of nucleation (which determines the number of filaments that are generated) and elongation (which dictates the lengths these filaments attain). I used this information to explore how tuning nucleation and elongation leads to the assembly of distinct actin filament populations (see Chapter 4).

To accurately measure filament numbers and lengths from individual TIRF micrographs, the program must recognize each filament as a discrete object. However, because filaments frequently overlap even in uncrowded imaging fields (Figure 6), this prerequisite is not easily met, thus leading to undercounts of filament numbers and overestimates of their lengths. Also, the extent of this bias varies across samples because images with more filaments and longer lengths are likely to have more overlaps.

To eliminate this bias, the program provides the user with the opportunity to resolve overlapping filaments. First, it automatically recognizes overlapping objects by their intersections, which MATLAB calls branchpoints (Figure 7). Next, the program highlights the first group of overlapping filaments and divides it into individual segments using intersections as breakpoints. The user then selects a segment and presses a key to specify whether the segment is a standalone filament or part of another filament (Figure 7). In this way, the user resolves overlapping filaments until the program has cycled through all of the flagged objects (Figure 8). It then calculates filament numbers and lengths using built-in MATLAB algorithms.

To evaluate the program's accuracy, I manually quantified filament numbers and lengths in three representative micrographs. Filament numbers measured using manual and semi-automated methods differed by an average of 2 ± 4 filaments, and the average difference in length was 0.65 ± 0.31 μm. Thus, my image analysis pipeline quickly and accurately quantifies filament numbers and lengths in actin populations imaged via TIRF microscopy. This expedited analysis made it possible to quantitatively dissect the balance between nucleation and elongation (see Chapter 4).

Automated Quantification of Bundle Assembly

My next goal was to quantify the assembly of actin bundles over time for reactions containing preassembled actin filaments and the crosslinker fascin. Because bundling produces a reproducible increase in the fluorescence signal along the lengths of actin filaments (Figure 9), the program identifies bundles by setting a threshold fluorescence intensity corresponding to the signal produced by two overlaid filaments. Different bundle thresholds can be set for different areas of the image, which is useful for images with uneven illumination. After thresholding, the program quantifies bundling using the following equation:

$$Fraction\ Bundled = \frac{F_{Bundled}}{F_{Total}} \quad (1)$$

where $F_{bundled}$ is the sum of individual pixel intensities above the set bundle threshold and F_{total} is the sum of all pixel intensities within skeletonized objects. This metric accounts for the incorporation of additional filaments into pre-existing bundles and also any variability in the total filamentous actin across imaging fields. To account for photobleaching, the program adjusts bundle intensity thresholds based on changes in single filament fluorescence over time. It also subtracts the average background

fluorescence from all fluorescence signal measurements to enable accurate comparisons across samples. For each bundling movie, I confirm the accuracy of bundle detection using visual representations of the analysis output (Figure 9).

After bundle quantification, the program generates bundling profiles by plotting the fraction of filamentous actin that is bundled over time. These plots have revealed that bundling proceeds in two distinct stages. The first stage involves an initial delay prior to the onset of bundling, whereas the second stage is characterized by bundle assembly. I fit time courses of the second stage in Kaleidagraph with the following single (2) or double (3) exponential equations:

$$Fraction\ Bundled = Ae^{-bt} + c \quad (2)$$

$$Fraction\ Bundled = A_1e^{-b_1t} + A_2e^{-b_2t} \quad (3)$$

where A represents the amplitude, b is the bundling rate, and c is the offset. I analyzed residuals to determine which equation to fit.

In this way, the MATLAB program automates bundle assembly quantification from TIRF microscopy movies and enables the extraction of bundling rates under a variety of different conditions, thus empowering my investigation into the filament length-dependence of fascin-mediated crosslinking (see Chapter 5).

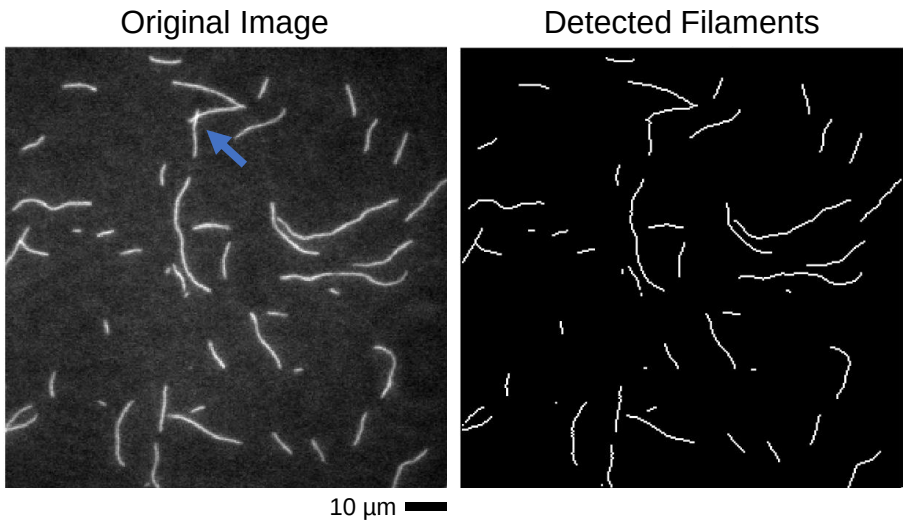

Figure 6. Skeletonized objects prior to overlap resolution. Representative image showing that the MATLAB program accurately detects actin filaments from TIRF micrographs. However, even uncrowded micrographs contain overlapping filaments (blue arrow), which could bias the quantification of filament numbers and lengths if they go unresolved.

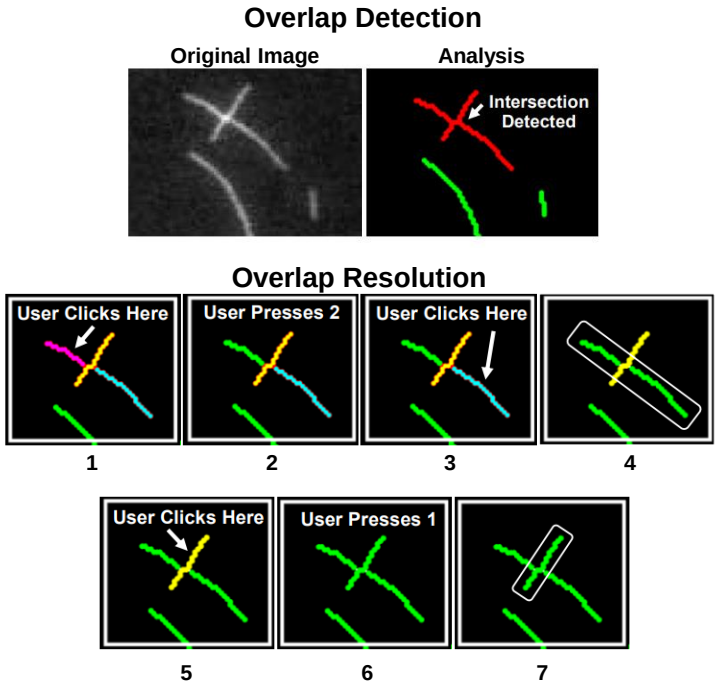

Figure 7. Automated detection and manual resolution of overlapping filaments. The program automatically detects overlapping filaments via their intersections ("branchpoints") and labels them in red. The program then cycles through overlapping filaments, and the user quickly resolves them. The lower panels show an example of this process. 1) Discrete segments are shown in different colors. The user clicks on a segment. 2) The segment is highlighted in green. The user presses 2 to indicate that the segment is part of another filament. 3) The user clicks the second segment of the two-part filament. 4) The segments are now recognized as part of the same filament (white box). 5) User clicks the remaining segment. 6) The user presses 1 to indicate the segment is a standalone filament. 7) The segment is now recognized as its own filament (white box).

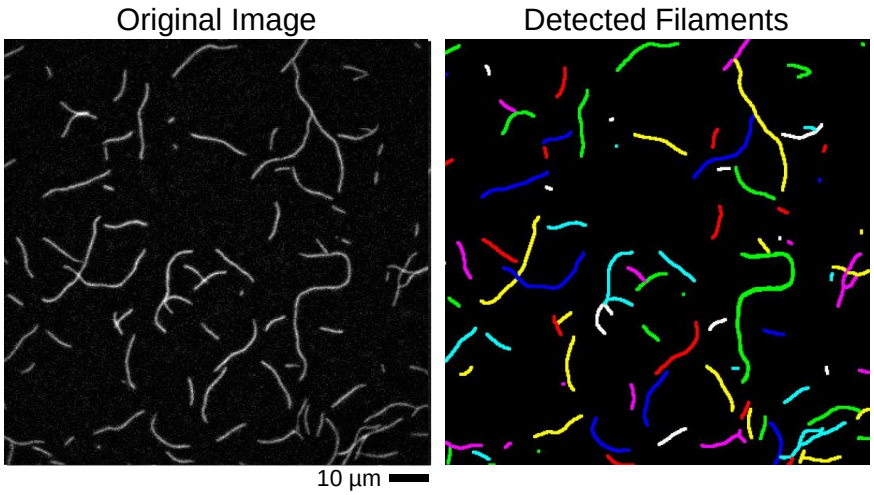

Figure 8. Most overlapping filaments can be resolved. A representative TIRF micrograph shown alongside the analysis output from MATLAB program. Objects recognized as individual filaments are displayed in different colors, illustrating that most overlapping filaments can be resolved. This minor, user-based intervention improves the accuracy of filament number and length quantification.

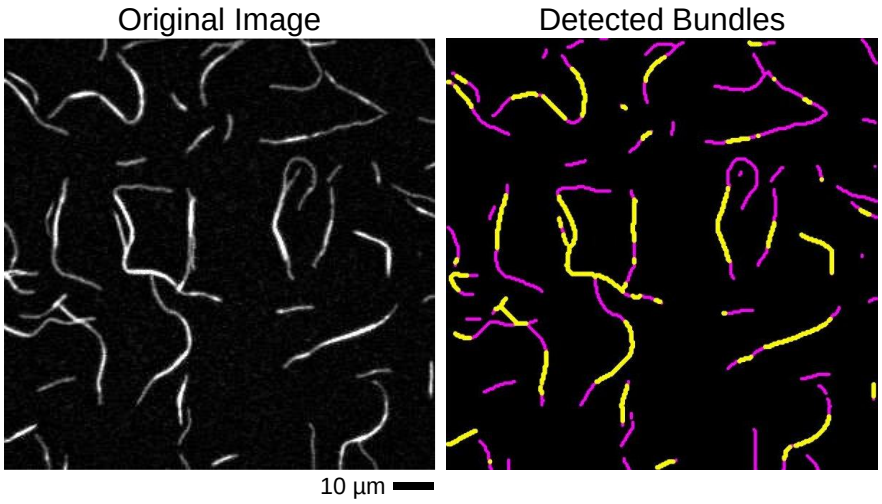

Figure 9. Accurate bundle detection. A representative TIRF micrograph from a bundle assembly movie shown alongside the analysis output from MATLAB program. Bundled regions are shown in yellow, and single filament regions are shown in magenta.

CHAPTER 4. Nucleation and Elongation to Actin Filament Assembly

Introduction

The proper functioning of higher-order actin structures depends on the cell's ability to control the composition of actin filament populations, which means assembling the correct number of filaments that are the appropriate length (Pfender et al., 2011; Chugh et al., 2017). These fundamental metrics are critically important because they dictate the mechanical and dynamic properties of actin structures. For example, longer filaments are more prone to bending and buckling than shorter filaments (Blanchoin et al., 2014). Also, filament numbers and lengths determine the rate of crosslinking and the establishment of different actin architectures (see Chapter 5) (Falzone et al., 2012, 2013).

Cells control filament numbers and lengths by regulating actin nucleation and elongation, which are mediated by actin-binding proteins like formins. In contrast to other actin nucleators or polymerases, formins carry out both processes, which they do by stabilizing actin nuclei and interacting with filament barbed ends in a profilin-dependent manner. When bound to the end of a filament, formin FH2 domains slow elongation by sterically interfering with incoming monomers and inducing conformational changes to the terminal actin subunits (Aydin et al., 2018). In the presence of profilin, formin FH1 domains bind to profilin-actin complexes and deliver monomers to barbed ends. This process overcomes FH2-mediated slowdowns in subunit addition, leading to faster filament elongation than free barbed ends (Courtemanche, 2018). Because of their multifunctionality, potency, and prevalence, formins are particularly important regulators of actin structure assembly (Table 1). As such, I focus specifically on formin-mediated nucleation and elongation in this chapter.

Because nucleation and elongation both consume actin monomers, these reactions necessarily compete with each other. This competition determines the number of actin filaments produced and the lengths filaments attain. If nucleation is significantly faster than elongation during actin polymerization, then monomers end up distributed across many filaments, resulting in short filament lengths at equilibrium (Figure 10). If elongation is faster, monomers are rapidly incorporated into pre-existing filaments, resulting in longer lengths. Fast elongation also depletes the pool of actin monomers, making nucleation less efficient and leading to fewer filaments.

Although it is known that nucleation and elongation compete, it remains unclear how formins dynamically balance these reactions to generate specific numbers of filaments that are the appropriate length for the construction of functional actin structures. Understanding this balance is difficult because it depends on the precise kinetics of multi-step, interrelated reactions that are further complicated by the mechanistic nuances of formins. To illustrate, formin-mediated polymerization includes the following steps: formation of actin nuclei, formin binding to nuclei, profilin binding to actin, profilin-actin binding to formin, FH1 delivery of profilin-actin to the barbed end, binding of profilin-actin to the barbed end, and binding of actin directly to either filament end (Zweifel et al., 2021). Historically, this complexity has made it challenging to quantitatively dissect formin-mediated nucleation and elongation.

However, advances in experimental methodologies and computational modeling have recently made it possible to investigate the interactions between these processes. In this study, I explored how formins balance nucleation and elongation to assemble specific filament populations. I polymerized actin filaments under different conditions to tune nucleation and elongation, and then I quantified the resulting filament numbers and lengths. To extract more information from the reaction outcomes, Dr. Mark Zweifel in the Courtemanche lab generated a kinetic model that captures each stage of actin filament

assembly with and without formins (Zweifel et al., 2021). Comparisons between the kinetic simulation and the experimental data shed light on understudied aspects of formin-mediated actin polymerization.

Results

To explore how the balance between nucleation and elongation influences the composition of actin filament populations, I carried out *in vitro* polymerization reactions with different formin isoforms and varying concentrations of actin and formin. Once the reactions reached equilibrium, I stabilized the assembled filaments with fluorescent phalloidin and visualized them via TIRF microscopy. Although reactions produced different numbers of filaments with different lengths, they all generated length distributions that were well-described by single exponential fits, which yields a single parameter than can be used to calculate the mean filament length and variance (see Methods)(Sept et al., 1999).

I first explored actin filament assembly under the simplest conditions. I excluded formin from these initial reactions and varied actin concentration (0. 75 - 2 µM), which affects the kinetics of both nucleation and elongation. However, the nucleation rate scales with the cube of the monomer concentration, whereas the elongation rate scales with the square (Zweifel et al., 2021). As a result, increasing the concentration of actin leads to more dramatic increases in filament nucleation rates than elongation rates, thus shifting the balance between these processes to favor nucleation.

The data show that reactions containing lower actin concentrations generate fewer filaments compared to reactions containing higher concentrations, which is consistent with inefficient nucleation at low monomer concentrations (Figure 11A,C). Average filament lengths are also longer for lower actin concentrations, which shows

that slow nucleation rates lead to the assembly of long filaments (Figure 11A,D). Dr. Zweifel's kinetic simulation closely tracks these experimental outcomes, indicating that it accurately reproduces spontaneous actin filament assembly (Figure 11C,D). Also, the average filament lengths for reactions containing 2 µM actin matched previous experimental observations (Sept et al., 1999), which suggests that our sample preparation prior to visualization minimizes filament shearing caused by pipetting (Figure 11B).

Next, I carried out actin assembly reactions containing a constant concentration of actin monomers (2 µM) and varying concentrations of the *S. pombe* formin Cdc12p. In the absence of profilin, Cdc12p slows down filament elongation by >99% (Kovar et al., 2003). Because Cdc12p largely prevents filament elongation, modulating its concentration allows me to titrate the effective nucleation rate without altering elongation. Inclusion of Cdc12p in polymerization reactions results in significantly more filaments than reactions without formin (Figure 12A-B). Increasing concentrations of Cdc12p lead to progressively more filaments until a plateau is reached around 250 nM. At this plateau, the Cdc12p samples contain over 10 times more filaments than the actin alone samples. Filaments assembled in these reactions are also much shorter than filaments assembled without formin (Figure 12C); average filament lengths plateau at 0.45 µm, which is >90% shorter than spontaneously polymerized filaments.

The kinetic model qualitatively reproduces these trends, but the shapes of the curves are much sharper in the model compared to the experimental data (Figure 13A-B). Since Cdc12p almost completely halts filament elongation, we hypothesized that this discrepancy is caused by factors related to formin-mediated nucleation, specifically the affinity of Cdc12p for actin nuclei, which has not been experimentally determined. The original value used in the kinetic model ($2*10^{-4}$ $\mu M^{-2}s^{-1}$) was from published work based off limited theoretical predictions (Paul and Pollard, 2008). To investigate whether this

parameter was the source of the discrepancy, we tested different values for the Cdc12p-actin nuclei association rate constant. Reducing the rate constant by a factor of ~3 ($0.7*10^{-4}$ $\mu M^{-2}s^{-1}$) produced simulated curves that better reflected the experimental data (Figure 13A-B).

Next, I added back in the complexity of filament elongation and carried out polymerization reactions with varying concentrations of the *S. cerevisiae* formin Bni1p. This formin allows filaments to elongate but slows down the rate by 50% compared to free barbed ends (Kovar et al., 2006; Paul and Pollard, 2008). Like Cdc12p, increasing concentrations of Bni1p lead to progressively more filaments and shorter filament lengths, until a plateau is reached above 500 nM Bni1p (Figure 12A-C). Compared to Cdc12p, Bni1p assembles fewer and longer filaments. At their respective plateaus, the number of filaments produced by Bni1p is ~3 times less than the number produced by Cdc12p, and these filaments are also ~2 times longer. Once again, the kinetic model reproduced these trends broadly, but the curve was much more dramatic in the simulation than *in vitro* (Figure 14A-B). Reducing the rate constant in the simulation by a factor of ~6 ($0.35*10^{-4}$ $\mu M^{-2}s^{-1}$) reproduced the experimental data much more closely.

Discussion

To investigate how formins balance nucleation and elongation to generate specific filament populations, I performed *in vitro* polymerization reactions and modulated the rates of nucleation and elongation by leveraging different formin isoforms and varying concentrations of actin and formin. I then quantified the resulting number of filaments and filament lengths.

I compared my experimental outcomes to Dr. Zweifel's computational model to learn more about formin-mediated filament assembly. The experimental data aligns well

with the simulated trendlines of filament lengths and numbers, thus confirming that the kinetic model is physiologically relevant. By fitting the model to the experimental data, we extracted the affinities of Cdc12p and Bni1p for actin nuclei, which have not been experimentally determined before. Our results indicate that Cdc12p's affinity for nuclei is about twice as strong as Bni1p's. More broadly, this method of estimating formin affinities for nuclei is useful for characterizing nucleation across different formin isoforms. Given that their actin assembly properties have been suggested to tailor formins to their specific cellular roles, this information will likely be key for understanding how different formin isoforms build distinct actin structures.

This work also provides insight into how cells optimize the balance between nucleation and elongation to generate distinct filament populations. The data show that increasing nucleation leads to a dramatic increase in the number of filaments at the expense of filament length. In contrast, elongation rates have a more limited effect on filament composition. Illustrating this point, reactions containing higher actin concentrations have faster elongation rates yet still produce shorter filaments. This outcome suggests that nucleation exerts a dominating influence over filament lengths and numbers.

To build actin structures like filopodia or stress fibers, cells need to assemble long actin filaments. The large impact of nucleation on filament composition suggests that reducing nucleation rates is a more efficient cellular strategy than increasing elongation rates. One way to reduce nucleation *in vitro* is to exclude formins. However, this is not an option in cells because formins protect filaments from capping protein (which completely prevents barbed end elongation). Cells also need formins to overcome the inhibition of nucleation by monomer-binding proteins like profilin. Instead, to make long filaments, cells express formins but keep their nucleation efficiency low. Therefore, formin autoinhibition plays a critical role in the assembly of long actin

filaments. In addition, when formin-mediated nucleation rates are low, it enhances the effect of elongation rate on filament length, thus allowing for formin isoforms with different elongation properties to tune filament lengths in actin populations.

In the next chapter, I utilize this insight on filament length control to probe how elongation affects the formation of crosslinked structures.

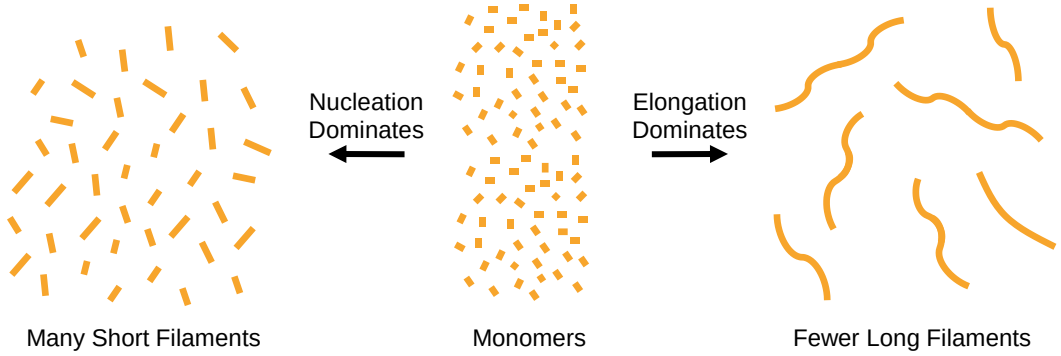

Figure 10. Nucleation and elongation determine filament lengths and numbers. If nucleation dominates, monomers are distributed across many filaments, resulting in short filament lengths. If elongation dominates, monomers are rapidly incorporated into pre-existing filaments, resulting in long filament lengths. This depletes the pool of actin monomers, making nucleation less efficient and leading to fewer filaments.

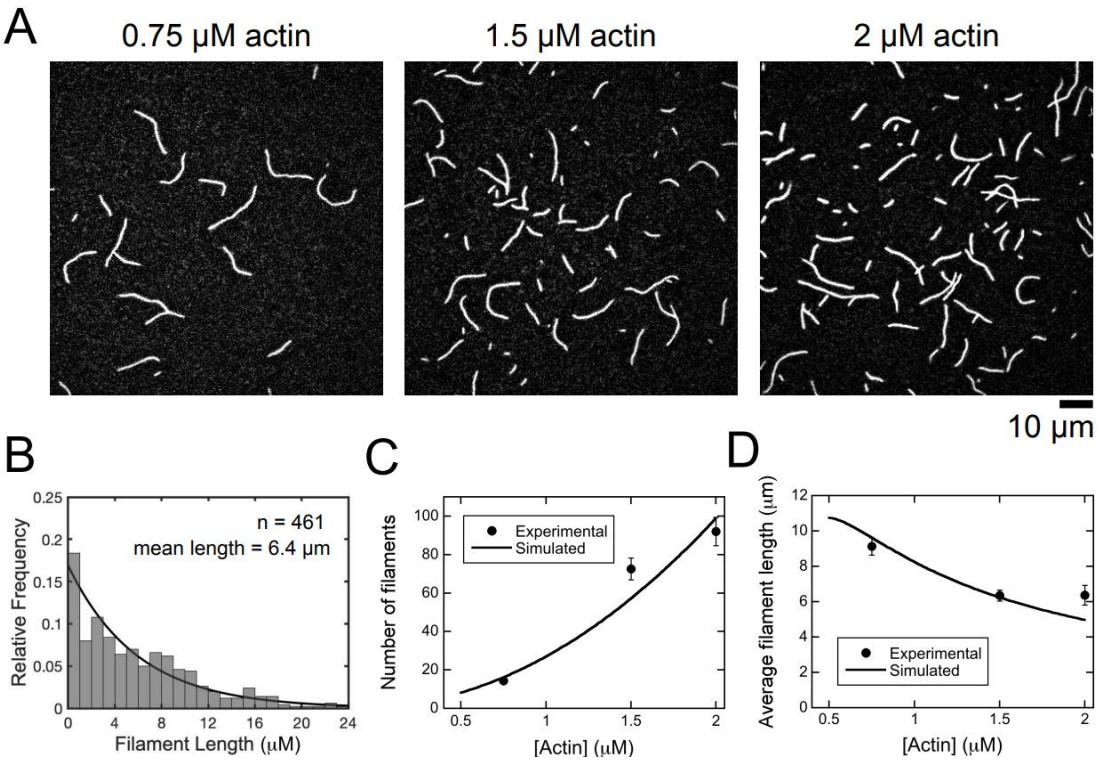

Figure 11. ***In vitro*** **actin polymerization in the absence of formin.** A range of actin monomers in polymerization buffer. The filaments were labeled with FITC-phalloidin and visualized by TIRF microscopy. **(A)** Representative TIRF micrographs of filaments assembled in reactions containing a range of actin concentrations. **(B)** Histogram of filament lengths measured at equilibrium for a representative polymerization reaction containing 2 μM actin. The line is an exponential fit to the data. The fitted value for λ is 0.156, and the mean filament length is 1/λ or 6.4 μm. **(C)** Dependence of the number of actin filaments visualized per 10,000 μm^2 on the actin concentration. Error bars are standard errors of the mean of at least 15 micrographs collected via three independent assays. Simulated data (solid line) were normalized and plotted on the same y axis scale as the experimental data. **(D)** Dependence of the average filament length on actin concentration. Error bars are standard errors of the mean of at least 15 micrographs collected via three independent assays. Simulated data (solid line) were normalized and plotted on the same y axis scale as the experimental data.

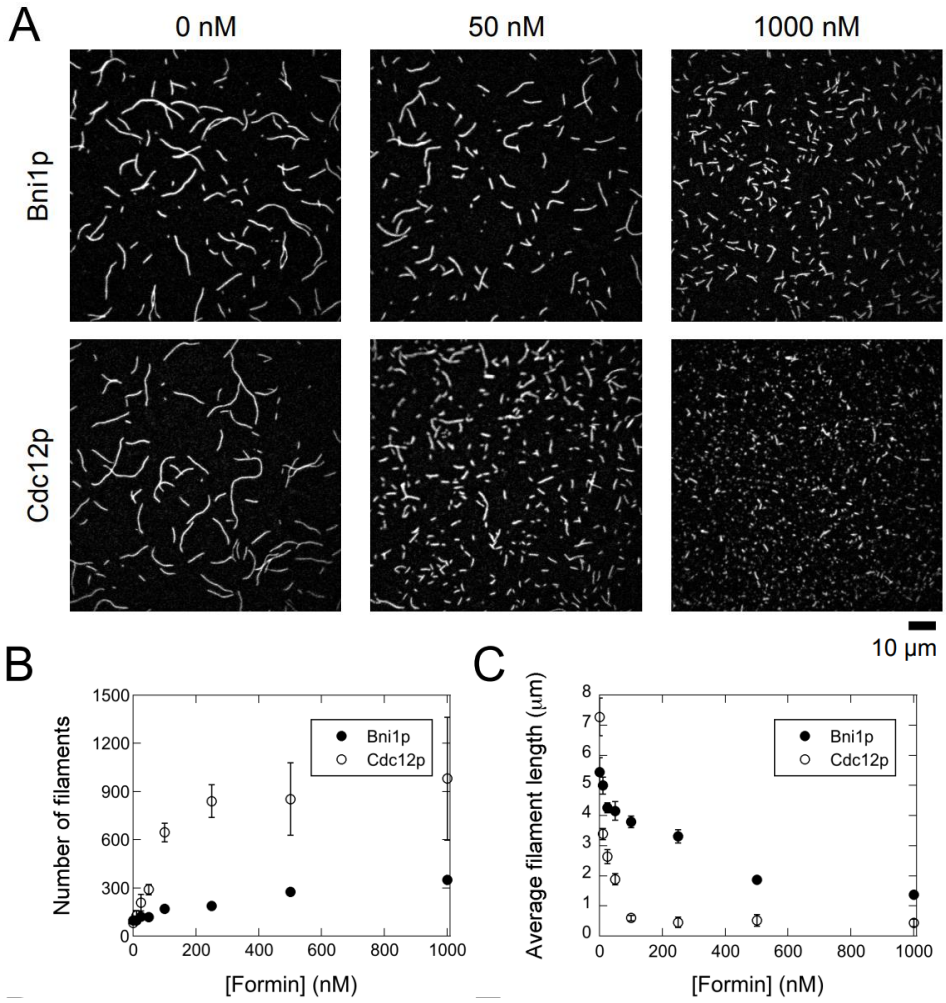

Figure 12. Bni1p and Cdc12p stimulate nucleation at the expense of filament length. 2 µM actin monomers and a range of concentrations of FH1FH2 constructs of Bni1p or Cdc12p in polymerization buffer. The filaments were labeled with FITC-phalloidin and visualized by TIRF microscopy. **(A)** Representative TIRF micrographs of filaments assembled in the absence and presence of Bni1p (top row) or Cdc12p (bottom row). **(B)** Dependence of the number of actin filaments visualized per 10,000 μm^2 on the concentration of Bni1p (solid circles) or Cdc12p (open circles). Error bars are standard errors of the mean of at least 15 micrographs collected via three independent assays.

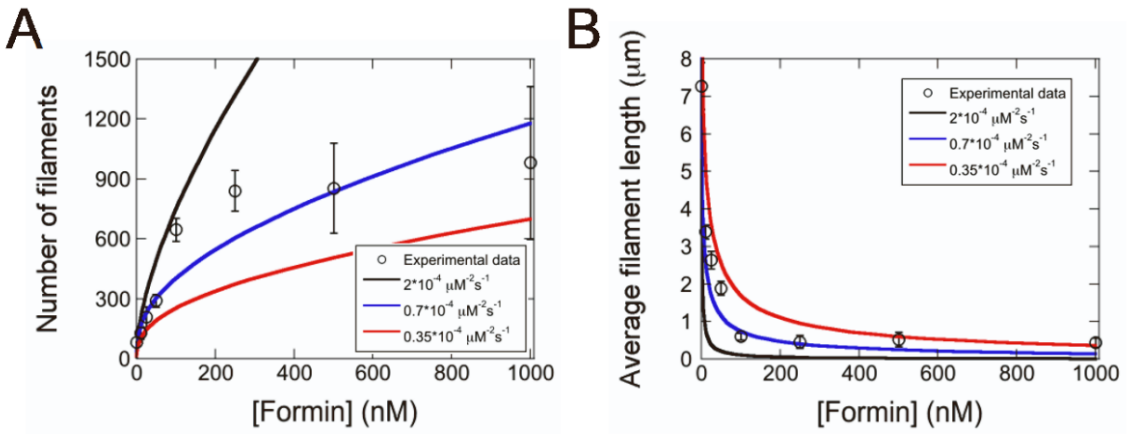

Figure 13. Comparison of experimental outcomes with computational modeling for reactions containing Cdc12p. The experimental conditions were as follows: 2 µM actin monomers and a range of concentrations of Cdc12p FH1FH2 in polymerization buffer. The filaments were labeled with FITC-phalloidin and visualized by TIRF microscopy**. (A and B)** Dependence of **(A)** the number of actin filaments visualized per 10,000 μm^2, or **(B)** the average filament length on the concentration of Cdc12p. Open circles are experimental measurements. Error bars are standard errors of the mean of at least 15 micrographs collected in 3 independent assays. Black and red lines are the simulated data. Simulations were performed using the published association rate constant for formin-mediated nucleation ($2*10^{-4}$ μM^{-2} s^{-1}; black lines), and rates that are approximately 3 and 6 times slower ($0.7*10^{-4}$ μM^{-2} s^{-1} and $0.35*10^{-4}$ μM^{-2} s^{-1}; blue and red lines).

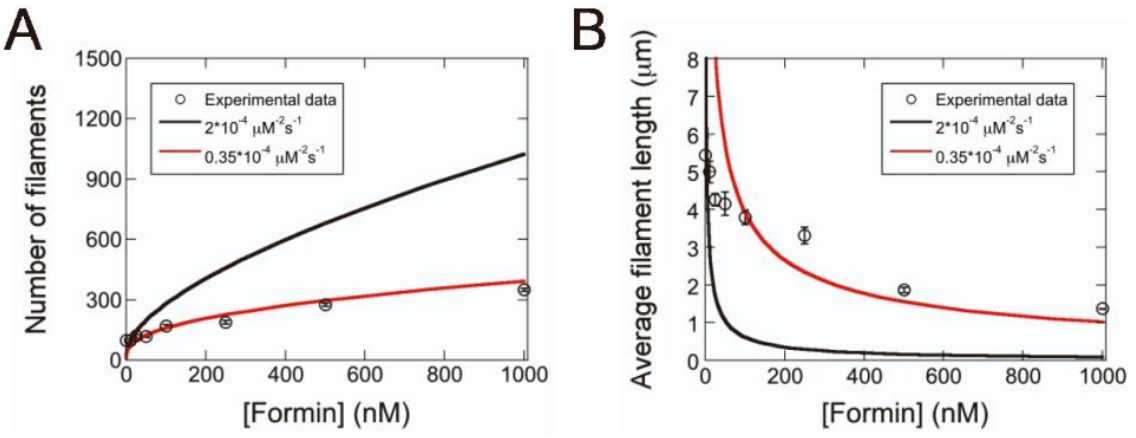

Figure 14. Comparison of experimental outcomes with computational modeling for reactions containing Bni1p. The experimental conditions were as follows: 2 µM actin monomers and a range of concentrations of Bni1p FH1FH2 in polymerization buffer. The filaments were labeled with FITC-phalloidin and visualized by TIRF microscopy. **(A and B)** Dependence of **(A)** the number of actin filaments visualized per 10,000 μm^2, or **(B)** the average filament length on the concentration of Bni1p. Open circles are the experimental measurements. Error bars are standard errors of the mean of at least 15 micrographs collected in 3 independent assays. Black and red lines are the simulated data. Simulations were performed using the published association rate constant for formin-mediated nucleation ($2*10^{-4}$ μM^{-2} s^{-1}; black lines) and a rate that is approximately 6 times slower ($0.35*10^{-4}$ μM^{-2} s^{-1}; red lines).

CHAPTER 5. Interdependence of Elongation and Fascin-Mediated Bundling in Crosslinked Structure Assembly

Introduction

The actin cytoskeleton dynamically assembles into discrete structures to support essential cellular functions, including motility, intracellular transport, and division. Construction of actin-based structures requires the polymerization of actin monomers into filaments, and the incorporation of these filaments into networks with precisely defined architectures (Blanchoin et al., 2014). The specific geometric arrangements of the filaments within actin structures are stabilized via the association of crosslinking proteins, which bind two filaments simultaneously (Michelot and Drubin, 2011; Blanchoin et al., 2014; Lappalainen, 2016; Pollard, 2016). The molecular properties of crosslinking proteins specify the filament spacing, orientation, and rotational freedom, and thus confer a unique set of mechanical properties to each structure (Bartles, 2000; Winkelman et al., 2016; Svitkina, 2018).

Crosslinking is a dynamic process that requires the assembly of actin filaments (Blanchoin et al., 2014). In the cellular environment, actin polymerization and crosslinking occur simultaneously (Mallavarapu and Mitchison, 1999; Vavylonis et al., 2006; Tang et al., 2015)), so these processes likely play interdependent roles in shaping the architectures and mechanical properties of actin-based structures. Recent studies have revealed that the rate at which actin filaments are generated influences the architecture of crosslinked networks assembled *in vitro* by alpha-actinin (Falzone et al., 2012, 2013). Alpha-actinin is a flexible crosslinker that assembles actin filaments into bundles that are characterized by a relatively wide inter-filament spacing of 35 nm and exhibit mixed polarity (Hampton et al., 2007). Increasing the rate of actin polymerization shifts the morphology of the structures generated by alpha-actinin from a population of sparse, thick bundles to a dense network of interconnected filaments (Falzone et al.,

2012, 2013). However, it remains unknown how the assembly of crosslinked actin structures evolves over the course of polymerization, and whether the length at which filaments initially become crosslinked influences the overall topology of the resultant actin network.

To answer these questions, we investigated how polymerization affects the assembly of simple, polarized actin bundles by the crosslinking protein fascin. Fascin is a monomeric actin-binding protein that localizes to protrusive cellular structures such as filopodia, invadopodia, and dendritic cell membrane extensions (Vignjevic et al., 2006; Li et al., 2010; Yamakita et al., 2011; Yang et al., 2013; Van Audenhove et al., 2016). These thin projections push against and deform the plasma membrane as they assemble and elongate outwards from the cell body (Mallavarapu and Mitchison, 1999), enabling them to play major roles in cellular motility, guidance, and invasion (Mattila and Lappalainen, 2008; Svitkina, 2018). The actin filaments that are assembled into protrusive structures are polymerized by formins and Ena/VASP family proteins (Schirenbeck et al., 2005; Breitsprecher et al., 2008; Lizárraga et al., 2009; Mellor, 2010; Jaiswal et al., 2013; Arthur et al., 2021). These filaments are assembled into ordered arrays by fascin, which bundles actin filaments by binding cooperatively along their lengths (Bryan and Kane, 1978; Yamashiro-Matsumura and Matsumura, 1985; Vignjevic et al., 2006). Fascin's compact three-dimensional structure specifies a relatively short inter-filament distance of 8 nm (Sedeh et al., 2010; Jansen et al., 2011), and its preference for binding filaments that are aligned in parallel orientations confers polarity to the bundles that it assembles *in vitro* (Courson and Rock, 2010). As a result, filament elongation primarily occurs at one end of each fascin-bound bundle (Jaiswal et al., 2013; Winkelman et al., 2014), consistent with the extension of protrusive structures in a single direction, away from the cell body. This topological feature facilitates direct measurement of bundle elongation within dynamically assembling filament networks.

Because protrusive structures elongate as they are assembled (Mallavarapu and Mitchison, 1999), we focused specifically on the effects of filament elongation on fascin-mediated bundling. Using a formin to generate populations of actin filaments of lengths representing distinct stages of elongation, we found that the rate of bundle assembly increases with filament length. We further observed that fascin assembles short filaments into topologically discrete bundles, whereas bundles of long filaments expand to form interconnected networks by incorporating additional filaments and forming stable, inter-bundle connections. Introducing actin monomers into reactions containing bundles of short filaments promotes their elongation and enables inter-bundle crosslinking. However, most connections formed between elongating bundles are short-lived and are followed by filament breakage at or near the initial site of crosslinking. Taken together, our data reveal that initiation of filament bundling early in elongation (i.e., when filaments are short) establishes a template that constrains the flexibility of the bundle. This increases the resistance of the bundle to changes in curvature that are required to form stable, interconnected networks. As a result, bundles of short filaments remain straighter as they elongate than bundles assembled from long filaments. Thus, uncoordinated filament elongation and crosslinking alters the morphology of actin bundles assembled by fascin, highlighting the importance of maintaining precise regulation of filament length during the assembly of specialized actin structures.

Results

Actin polymerization and bundling are dynamic reactions that take place simultaneously during the assembly of higher-order actin structures (Mallavarapu and Mitchison, 1999; Vavylonis et al., 2006; Tang et al., 2015). As a result, monitoring the progress of each reaction is complicated by contributions from the other. To investigate the effects of

filament elongation on the mechanism of fascin-mediated bundling, we sought to simplify our reactions by systematically controlling the progress of the elongation reaction. To do so, we used a formin to assemble populations of actin filaments with defined lengths. We used these preassembled filaments to represent progressive stages of elongation, with longer filaments representing later time points.

We selected the fission yeast formin Cdc12p as a representative formin for our assays because it decreases the filament elongation rate by 99% in the absence of profilin (Kovar et al., 2003, 2006). The extremely slow elongation of filaments bound by Cdc12p enables us to directly control filament length by modulating the concentrations of actin and formin (Zweifel et al., 2021). Importantly, unlike the mammalian formins FHOD1 and mDia2, which also possess slow elongation activities, and Daam1 and FMNL2, which polymerize actin filaments that are incorporated into protrusive structures (Harris et al., 2006; Esue et al., 2008; Jaiswal et al., 2013; Schönichen et al., 2013), Cdc12p does not bundle or bind along the lengths of actin filaments when present at concentrations exceeding 100 nM (Scott et al., 2011). Cdc12p is therefore ideally suited for our assays, which require relatively high formin concentrations to generate short actin filaments.

To assemble filaments with different lengths, we incubated purified actin monomers in polymerization conditions in the absence and presence of a construct containing the two major actin polymerization domains of Cdc12p (i.e., the FH1 and FH2 domains) (Kovar et al., 2003). Like most formins, Cdc12p nucleates filaments by encircling and stabilizing dimers and trimers of actin monomers with its dimeric FH2 domain (Pring et al., 2003; Moseley et al., 2004; Otomo et al., 2005; Lu et al., 2007; Yamashita et al., 2007). Following nucleation, the FH2 dimer steps onto incoming actin subunits to incorporate them into the filament, thus enabling the formin to remain processively bound at the barbed end of the elongating filament (Courtemanche, 2018).

Once each polymerization reaction reached equilibrium, we added fluorescent phalloidin, imaged the filaments using total internal reflection fluorescence (TIRF) microscopy, and quantified their lengths. We found that each reaction robustly assembled into filaments of varying lengths (Figure 15A). The distributions of filaments lengths are well characterized by single exponential fits (Figure 15B), which yield an average filament length and a variance (see Methods).

In the absence of formin, we measured an average filament length of 7.0 μm, in agreement with published measurements performed on similar reactions (Sept et al., 1999; Zweifel et al., 2021) (Figure 15B, Actin alone). Addition of Cdc12p following polymerization does not significantly alter the average filament length (Figure 15B, Cdc12p-bound), confirming that formins do not influence the lengths of preassembled actin filaments. In contrast, inclusion of Cdc12p at the time of initiation of polymerization dramatically increases the number of actin filaments assembled over the course of the reaction (Supplementary Figure S1). This increase in filament nucleation is matched by a narrower length distribution that is significantly shifted toward short lengths (1.3 μm average length) (Figure 15B, Cdc12p-assembled).

Fascin binds with similar affinity to short and long actin filaments

Formin binding has been shown to alter the conformation of the subunits at the barbed ends of actin filaments (Aydin et al., 2018). This structural effect propagates at least 200 nm along the length of the filament and is proposed to influence the association of other actin-binding proteins, including tropomyosin and cofilin (Bugyi et al., 2006; Papp et al., 2006; Skau et al., 2009; Johnson et al., 2014; Mizuno et al., 2018). To determine if binding of Cdc12p to the barbed ends of actin filaments alters fascin's actin-binding and bundling activities, we performed low-speed co-sedimentation assays with each of our

populations of filaments. We found that saturating concentrations of fascin efficiently bundle actin filaments that are polymerized both in the absence and presence of formin (72 ± 3% and 73 ± 3% of the total filamentous actin is incorporated into bundles in the absence and presence of formin, respectively) (Supplementary Figure S2). As previously reported, fascin binds cooperatively to actin filaments with free (i.e., not formin-bound) barbed ends with a dissociation constant of 396 $\pm$ 36 nM (Figure 15C, Actin alone) (Jansen et al., 2011; Winkelman et al., 2016). Fascin also binds cooperatively to short and long Cdc12p-bound filaments with similar affinities (K_d = 431 $\pm$ 43 nM and 303 $\pm$ 110 nM), indicating that Cdc12p does not alter fascin's equilibrium actin-binding or bundling activities (Figure 15C, Cdc12p-assembled, Cdc12p-bound). Binding of phalloidin to actin filaments also does not alter fascin's binding affinity (Supplementary Figure S3).

Fascin bundles short and long filaments cooperatively

Fascin's cooperative interactions with actin filaments indicate that an initial binding event increases the probability of subsequent fascin binding at a neighboring site. This is consistent with the observation that fascin-mediated bundling causes filaments to "zipper" together as binding propagates along the lengths of filaments (Breitsprecher et al., 2011). To determine how filament length influences this cooperative binding process, we visualized fascin-mediated bundling in real-time using TIRF microscopy. Because Cdc12p does not alter fascin's affinity for actin filaments, we omitted Cdc12p from reactions containing long filaments. The absence of formin in these samples enables filament annealing during sample preparation, which helps to maintain consistent filament length and maximizes differences among samples containing short and long

filaments. To mimic a single population of actin filaments at distinct stages of elongation, we used equal concentrations of short and long filaments in our reactions.

Fascin-mediated bundling requires an initial alignment of two filaments into a parallel orientation and at an inter-filament distance that promotes stable binding of fascin (Courson and Rock, 2010). By observing individual bundling events, we found that alignment often occurs along short stretches of filaments that encounter one another at an angle (Figure 16A,B). By measuring the angles at which filaments encounter one another prior to bundle formation, we found that short filaments must be aligned in a nearly parallel orientation to promote bundling (Figure 16C; average angle of alignment of 14.4º). In contrast, we observed a much larger variation in the relative orientation of long filaments that undergo bundling (Figure 16D; average angle of alignment of 65.5º), consistent with a length-dependent increase in filament flexibility.

Following filament alignment, fascin-mediated bundling produces a quantifiable increase in the fluorescence signal along the lengths of actin filaments (Figure 16A) (Breitsprecher et al., 2011). As each reaction progresses, changes in fluorescence intensity occur along the lengths of crosslinked filaments until bundling is complete and sequential micrographs reveal no further changes.

At equilibrium, bundles assembled from both short and long filaments contain a mixture of crosslinked regions consisting of multiple overlapping filaments, and regions corresponding to stretches of single filaments that contain no crosslinks (Figure 16F, left panels). Bundles also exhibit variable curvature along their lengths. To assay for length-dependent differences in curvature, we measured bundle tortuosity by dividing the contour length of each bundle by its end-to-end distance (Figure 16E). We found that bundles of short filaments exhibit less tortuosity, and are therefore straighter, than bundles of long filaments.

To quantify crosslinking along the lengths of actin bundles, we employed a computational analysis tool developed in-house that uses fluorescence intensity to detect single and overlapping stretches of actin filaments (see Methods) (Figure 16F, right panels). We determined that crosslinked regions comprise ~70% of the total length of actin bundles at equilibrium (Figure 16G). This structural feature is insensitive to both filament length and fascin concentration, suggesting that this is a general property of actin bundles assembled by fascin.

Fascin-mediated bundling occurs via distinct phases

To investigate the effects of filament length on the rate of bundle assembly, we quantified the fraction of filamentous actin that is crosslinked over the course of reactions containing either short or long filaments (Figure 17A,B). For both populations, we observed a delay between the addition of fascin and the onset of bundling. The length of this delay decreases as the fascin concentration increases, until a plateau is reached at 500 nM fascin (Figure 17C). This indicates that the initiation of bundling depends on the rate at which fascin binds actin. The delay is insensitive to filament length, except at the lowest sampled fascin concentration, suggesting that filament length does not influence the rate at which fascin binding is initiated.

Following the initial delay, the fraction of actin that is bundled increases over time until a plateau is reached (Figure 17B). Bundling profiles collected at fascin concentrations up to 500 nM (which corresponds to ~60% saturation of the available binding sites) are well described by single exponential functions, independent of filament length (Figure 18A). Thus, at these concentrations of fascin, bundling occurs in a single kinetic phase. The rate constants generated by fits to the data reveal that reactions containing short filaments are bundled more slowly than reactions containing long

filaments (Figure 18B). Bundling rates measured in reactions containing long filaments are more variable than those obtained with short filaments. The magnitude of this variability is directly proportional to the variance in the lengths of the filaments in our populations of short and long filaments. Despite the increased variability observed in reactions containing long filaments, the differences between the bundling rates for short and long filaments are statistically significant across all fascin concentrations (Welch's t-test; $p<0.03$), except for the lowest sampled concentration.

At concentrations exceeding 500 nM fascin, bundling of short filaments remains well described by a single exponential function (Figure 18C). However, fitting bundling profiles for long filaments requires a double exponential function, revealing the emergence of a second kinetic bundling phase.

An increase in filament length promotes bundle expansion

Bulk bundling reactions contain numerous filaments that progress through bundle assembly at different times (Figure 17A). This asynchrony can lead to temporal overlap of otherwise discrete bundling phases, complicating their resolution. To determine the origin of the two bundling phases in our reactions with long filaments, we therefore examined the different types of bundling events that take place in the presence of a saturating concentration of fascin (i.e., 1400 nM fascin). We first quantified the rate of *de novo* bundle formation in our reactions. Formation of new bundles involves the crosslinking of two individual filaments together and excludes bundle "expansion" events, in which pre-existing bundles incorporate additional filaments. Consistent with our bulk bundling measurements (Figure 17B), we found that the number of new bundles increases over the course of the reaction (Figure 18D). Fitting the data with single exponential functions reveals that new bundle formation is slower for short filaments

than for long filaments (0.002 s^{-1} and 0.003 s^{-1}, respectively). Notably, the assembly of new bundles in reactions containing long filaments is completed within ~1000 s, matching the length of the first exponential phase observed in our bulk bundling measurements (Figure 18C, Long filaments). This suggests that the first phase of bundle assembly corresponds to the formation of new bundles.

In reactions containing 1400 nM fascin, bundling of long filaments continues after the assembly of new bundles is complete (Figure 18C, Long filaments). To determine the mechanism driving this continuation of the bundling reaction, we compared micrographs collected at various time points over the course of the first and second exponential phases (Figure 19A). We found that bundling that occurs early in the first phase (~500 s) is characterized by the formation of new bundles. These early bundles tend to have linear morphologies (defined by the presence of two bundle ends) and a single continuous crosslinked region. Toward the end of the first phase (~900 s), most of the single actin filaments have been incorporated into bundles. In contrast, bundles observed during the second phase often contain more than two filaments, multiple crosslinked regions, and branched morphologies (defined by the presence of more than two bundle ends), suggesting that discrete bundles become interconnected by merging together during the second phase (Figure 19A, arrows, asterisks).

When individual filaments become crosslinked into bundles, the number of discrete filamentous structures contained in the reaction decreases. This number further decreases as bundles expand by incorporating additional filaments or coalesce with other preassembled bundles (Figure 19B). To assess the contributions of bundle expansion to the kinetics of bulk bundling reactions, we measured the number of filamentous structures (i.e., the sum of the individual actin filaments and filament bundles) present in our reactions as bundling progresses. In reactions that undergo bundling in a single kinetic phase, we found that the number of filamentous structures

decreases as the reaction proceeds and reaches a plateau at approximately 60% of the initial number of structures (Figure 19C). The magnitude of this change is similar in samples containing short and long filaments, indicating that, at equilibrium, each filamentous structure contains approximately two filaments. This is consistent with the absence of a distinct bundle expansion phase.

In the presence of 1400 nM fascin, the number of filamentous structures observed in reactions containing short and long filaments decreases at similar rates and with the same magnitude until the end of the first phase (~1000 s) (Figure 19D). At longer times, the number of structures remains unchanged for short filaments but continues to decrease until a plateau is reached at approximately 30% of the initial number of structures in reactions containing long filaments. This value indicates that the assembled bundles contain more than two filaments on average, thus supporting a model for bundle expansion in reactions containing long filaments.

To assess the effects of bundle expansion on the overall morphology of bundled actin networks, we quantified the number of filamentous structures in reactions that have reached equilibrium as a function of the concentration of fascin (Figure 19E). We found that bundling decreases the number of filamentous structures by 30-50% in reactions containing short filaments, corresponding to an average of two or fewer actin filaments per structure. Reactions containing long filaments assemble into a similar number of filamentous structures at concentrations of fascin below 150 nM. At higher fascin concentrations, long filaments assemble into a smaller number of structures than do short filaments.

Despite the absence of a distinct bundle expansion phase, bundles of short filaments occasionally incorporate additional filaments or merge with other bundles over the course of our reactions. These expansion events require the alignment of merging bundles into a nearly parallel orientation (Figure 19F; average angle of alignment of

16.8º). As a result, short filament bundles retain linear morphologies following expansion. In contrast, bundles of long filaments can form inter-bundle crosslinks when oriented at a wide range of angles, thereby promoting the assembly of branched bundles (Figure 19G; average angle of alignment of 86.6º). Taken together, our results indicate that fascin crosslinks short filaments into bundles that remain linear and discrete over the course of the reaction, whereas bundles of long filaments coalesce into interconnected networks with irregular morphologies.

Bundles of Short Filaments Remain Discrete While Elongating

The results of our experiments with short and long actin filaments suggest that filament length plays a central role in regulating bundle assembly by dictating the probability of forming interconnections between bundles. To determine how the length at which filaments initially become crosslinked impacts the architecture of dynamic actin networks, we investigated whether filament elongation can alter the organization of preassembled actin bundles. We introduced actin monomers and fascin into reactions containing bundles of short, Cdc12p-bound filaments and visualized elongation using TIRF microscopy. To promote Cdc12p-mediated filament elongation and inhibit spontaneous filament nucleation, we included 10 µM profilin in each reaction. Profilin is a cytoplasmic protein that binds actin monomers and sterically hinders the inter-monomer associations that are necessary for filament nucleation (Pollard and Cooper, 1984). Binding of profilin-actin complexes to polyproline tracts located in formin FH1 domains promotes their delivery to the barbed end, where they are incorporated into the filament via stepping of the FH2 domain (Courtemanche, 2018).

Following the addition of actin monomers and profilin, preassembled bundles elongate at only one end (Figure 20A, arrows), reflecting the parallel orientation of

filaments bundled by fascin. The growing ends of bundles appear dimmer than the rest of the bundle owing to the lower fluorescence intensity of filaments assembled by formins from Oregon green-labeled monomers and profilin (Sherer et al., 2018) compared to FITC-phalloidin-labeled filaments. This feature facilitates the identification of each bundle's barbed end and enables us to track the relative orientation of each bundle over time. Preassembled bundles elongate approximately half as fast as single filaments in identical polymerization conditions (Figure 20B) (Zweifel and Courtemanche, 2020), consistent with published reports of the inhibitory effects of bundling on polymerization (Suzuki et al., 2020).

As we observed in reactions containing single filaments, we found that elongating bundles occasionally establish interconnections with other bundles (Figure 20A, asterisks). Doubling the concentration of actin monomers doubles the elongation rate and decreases the length of the delay between the initiation of bundle elongation and the formation of the first inter-bundle connection by ~50% (Figure 20B,C). Following the formation of the first inter-bundle connection, elongating bundles continue to merge with one another until equilibrium is reached. The rate at which these inter-bundle connections form increases with the filament elongation rate (Supplementary Figure S4A). However, many of these connections are transient and break as elongation and crosslinking progress (Figure 20D). These "unstable" connections form between elongating bundles that are oriented at a wide range of angles (Figure 20E, Unstable connections). To distinguish transient connections from long-lived binding events that ultimately alter the architecture of the bundled actin network, we classify connections that persist without breaking over the course of our bundling reactions as "stable". Whereas 95% of the inter-bundle connections that form in reactions containing non-elongating filaments are stable, only 69% of the connections formed between elongating preassembled bundles are stable. These long-lived connections are established

between elongating bundles that are oriented into a relatively narrow range of angles (Figure 20E, Stable connections). These angles are more acute, and are therefore closer to a parallel orientation, than those observed during the expansion phase in reactions containing long single filaments (Figure 19G). As a result, the establishment of stable connections gives rise to networks containing large, straight bundles that exhibit less curvature than bundles formed in reactions containing individual, long filaments (Figure 20F).

The rate at which unstable, transient connections form increases with the filament elongation rate (Supplementary Figure S4B). In contrast, the rate at which stable inter-bundle connections form is insensitive to the rate of elongation and matches the rate at which non-elongating, short bundles form inter-bundle connections (Figure 20G). This rate is approximately 60% slower than the rate at which long filament bundles form inter-bundle connections. As a result, reactions containing actin bundles that are preassembled from short filaments contain a larger number of discrete bundles than do reactions containing long filaments, despite attaining similar filament lengths via elongation.

Discussion

The construction of higher-order actin structures requires the polymerization and crosslinking of actin filaments into networks with specific architectures (Blanchoin et al., 2014). To understand how the process of filament elongation regulates the dynamic assembly of polarized actin bundles, we examined the effects of filament length on fascin-mediated bundling. We found that filament length directly influences both the rate of bundle formation and the likelihood that discrete bundles will expand and merge to form interconnected networks.

A model for length-dependent filament bundling

Based on our quantifications of filament bundling reactions, we propose that bundling occurs via two distinct phases (Figure 21). During the first phase, individual filaments become crosslinked together to form new bundles. During the second phase, pre-existing bundles expand by incorporating additional filaments and merging with other bundles. Our data suggest that the bundle formation phase dominates reactions containing either short filaments or sub-saturating concentrations of fascin (Figures 18 and 19). The rate of bundle formation increases with filament length, suggesting that the rate of filament elongation might regulate this process. The limited contribution of bundle expansion to these reactions enables the formation of discrete bundles that contain few filaments. In contrast, bundles assembled from long filaments undergo significant expansion by incorporating additional filaments and merging with one another in the presence of fascin concentrations exceeding 250 nM (corresponding to >25% saturation of the available fascin binding sites). This process leads to bundle thickening and shifts the architecture of the bundles into an interconnected network. By comparing the number of filamentous structures prior to and following bundling, we found that reactions containing long filaments undergo bundle expansion in the presence of 250-500 nM fascin despite the absence of a distinct second kinetic bundling phase. This suggests that bundle formation and expansion progress at similar rates in these reactions, in contrast to the relatively fast rates of bundle formation and slower rates of bundle expansion we observe at saturating fascin concentrations.

The persistence length of actin filaments (10 μm (Isambert et al., 1995; McCullough et al., 2008)) is likely a key determinant of bundling propensity. Whereas short filaments are relatively straight, long filaments are more likely to exhibit curvature

and thus sample a range of conformations. This increased flexibility facilitates the alignment of stretches of filaments into orientations that are compatible for bundling (Figure 16D), thereby speeding bundle formation (Figure 18B). Following initial bundle assembly, incorporation of additional filaments into pre-existing bundles depends on the probability that two filamentous structures will become aligned in an orientation that is compatible for bundling. This probability increases with filament length as the range of angles into which filamentous structures can be oriented to promote bundling also increases (Figures 19F,G).

We found that stretches of single filaments lacking crosslinks are typically located at bundle ends and comprise approximately 30% of the total length of each bundle (Figure 16G). As a result, bundles of long filaments possess longer stretches of single filaments than bundles of short filaments. As with bundle formation, the length of these regions likely dictates the probability that they will contact other filaments or bundles at orientations that are compatible for fascin binding. Thus, longer stretches of single filaments promote bundle expansion. On the other hand, the presence of short stretches of single filaments indicates that the barbed ends of the bundled filaments are in relatively close spatial proximity to one another. This alignment of the filaments likely imparts uniform structural rigidity along the length of elongating bundles, thus enabling protrusive structures to withstand compression as they deform the plasma membrane and assemble outward from the cell body.

Filament length at the onset of bundling influences the architecture of bundled actin networks

To determine whether the lengths at which filaments initially become crosslinked constrains the architecture of dynamically elongating networks, we visualized changes in

the morphologies of preassembled bundles of Cdc12p-bound short filaments under polymerization conditions. We found that bundles elongate unidirectionally and occasionally become crosslinked with neighboring bundles. We determined that the length of time required to establish the first inter-bundle connection is inversely dependent on the elongation rate. Following this initial inter-bundle crosslinking event, subsequent connections form among other elongating bundles. The rate at which these connections are formed also positively correlates with the elongation rate but is slower than the rate measured in reactions containing long single filaments (Supplementary Figure S4A).

Approximately one third of the connections formed between elongating bundles are short-lived and are followed by filament breakage at or near the initial site of crosslinking (Figure 20D). Since fascin is an inflexible crosslinker that assembles rigid bundles (Claessens et al., 2006; Van Audenhove et al., 2016), the breakage of these short-lived connections is likely caused by geometric constraints imposed by fascin-mediated crosslinking. Based on our observations, we classified connections that persist throughout our reactions as “stable.” These connections are formed following the alignment of bundles into a narrow range of acute angles, which promotes the retention of bundle linearity following their coalescence. Thus, although filament elongation enables the formation of inter-bundle connections, our data suggest that crosslinking early in elongation pre-aligns growing filaments, setting a template for continued bundle assembly as elongation proceeds. This initial alignment constrains the flexibility of the bundled filaments, increases their resistance to large changes in curvature and inhibits their coalescence into interconnected networks with branched morphologies. As a result, preassembled bundles of short filaments remain straighter following elongation than bundles assembled from long filaments of the same length (Figure 20F).

Physiological implications of a length-dependent mechanism that regulates the architecture of crosslinked actin networks

The specialized architectures of higher-order actin structures dictate their rigidity, mechanosensitivity, contractility, and lifetime (Reymann et al., 2012; Gressin et al., 2015; Ennomani et al., 2016; Chugh et al., 2017; Stam et al., 2017; Ajeti et al., 2019). These physical properties enable actin structures to perform specific biological functions and must therefore be tightly regulated. We have found that uncoordinated filament elongation and crosslinking can alter the architecture of bundled actin networks assembled by fascin, thus highlighting the importance of filament length regulation during the assembly of protrusive actin structures.

In cells, a large fraction of the filaments that are incorporated into bundled actin structures are polymerized by formins (Schirenbeck et al., 2005; Lizárraga et al., 2009; Mellor, 2010; Jaiswal et al., 2013). Most eukaryotes express at least two formin isoforms, which nucleate and direct the elongation of actin filaments at a wide range of isoform-specific rates (Schönichen and Geyer, 2010; Pruyne, 2016). Our results suggest that the elongation properties of formin isoforms likely play a central role in the precise incorporation of actin filaments into structures with specific architectures by controlling the rate of change in filament length. Similarly, the association rate and structural properties of the crosslinking protein are also determinants of actin network architecture (Bartles, 2000; Winkelman et al., 2016; Svitkina, 2018). For example, flexible crosslinkers like α-actinin and filamin A are less sensitive to the relative alignment and orientations of actin filaments than are rigid crosslinkers like fascin (Popowicz et al., 2006; Sjöblom et al., 2008; Courson and Rock, 2010). These crosslinkers may therefore facilitate the formation of a larger number of stable connections among elongating

bundles than we observed using fascin. This would enable filament elongation to transform disconnected bundles into interlinked networks.

Perturbation of the expression levels of regulators of actin filament length has been shown to disrupt the assembly and functions of several bundled actin structures in cells. For example, in budding yeast, deletion of the myosin passenger protein Smy1p, which binds and slows polymerization mediated by the formin Bnr1p, results in an increase in actin cable length and curvature (Chesarone-Cataldo et al., 2011). Simulations of actin cable assembly have revealed that this phenotype arises from an increase in inter-cable connections that form when the rate of filament polymerization is abnormally fast (Tang et al., 2015). In fission yeast, cytokinetic contractile ring assembly proceeds via a “search-capture-pull” mechanism in which formins localize to large protein assemblies called “nodes” and polymerize actin filaments (Vavylonis et al., 2008). Myosin-II in neighboring nodes binds and pulls on the actin filaments, leading to the formation of a uniform, contractile actomyosin ring. Disruption of cofilin-mediated actin filament severing produces an abnormal clumping of nodes during cytokinetic ring assembly (Chen and Pollard, 2011). This phenotype is similar to the defects observed when the number of long-lived inter-filament connections is increased in simulations of contractile ring assembly. Thus, filament length regulation through severing is required to disassemble improper inter-filament crosslinks that otherwise disrupt the architectural integrity of contractile rings. Finally, depletion of capping protein, which binds and inhibits the elongation of actin filaments, increases the thickness of the actin cortex in HeLa cells. In contrast, depletion of the formin Dia1 decreases actin cortex thickness (Chugh et al., 2017). In both cases, cortical actin tension decreases during mitosis, consistent with a mechanism that ensures that maximum cortical tension is achieved at intermediate filament lengths.

Modulating the expression levels and activities of crosslinkers also leads to anomalies in actin structure formation and function. For example, cells expressing a mutant version of fimbrin (Sac6p) that has a weakened affinity for actin filaments assemble shorter and fewer actin cables in budding yeast despite normal rates of filament elongation by formins (Miao et al., 2016). This phenotype may arise from a delay in fimbrin-mediated crosslinking, which would lead to the formation of aberrant inter-filament connections and the assembly of meshworks of long actin filaments rather than the discrete bundles that are characteristic of wildtype actin cables.

RNAi-induced silencing of fascin decreases the number of filopodia that are assembled in mouse melanoma cells (Vignjevic et al., 2006; Jaiswal et al., 2013). These filopodia exhibit a “wavy” morphology, suggesting a reduction of mechanical stiffness (Vignjevic et al., 2006; Jaiswal et al., 2013). Similarly, knockdown of fascin in the human melanoma cell line CHL-1 decreases the number, length, and lifetime of invadopodia and reduces the matrix degradation activity of these protrusions (Li et al., 2010). In both cases, limited fascin availability may delay filament crosslinking and decrease the stiffness of growing actin bundles, causing filament elongation to stall. In this way, disruption of the interdependent kinetics of filament elongation and crosslinking during the assembly of filopodia and invadopodia may therefore provide a molecular mechanism by which downregulation of fascin expression decreases the probability of cancer metastasis (Weaver, 2006; Jacquemet et al., 2015). On the other hand, the high fascin expression levels that are often associated with aggressive metastatic cancers (Hashimoto et al., 2005) may guarantee filament crosslinking early in elongation, thus promoting the robust assembly of invasive actin protrusions.

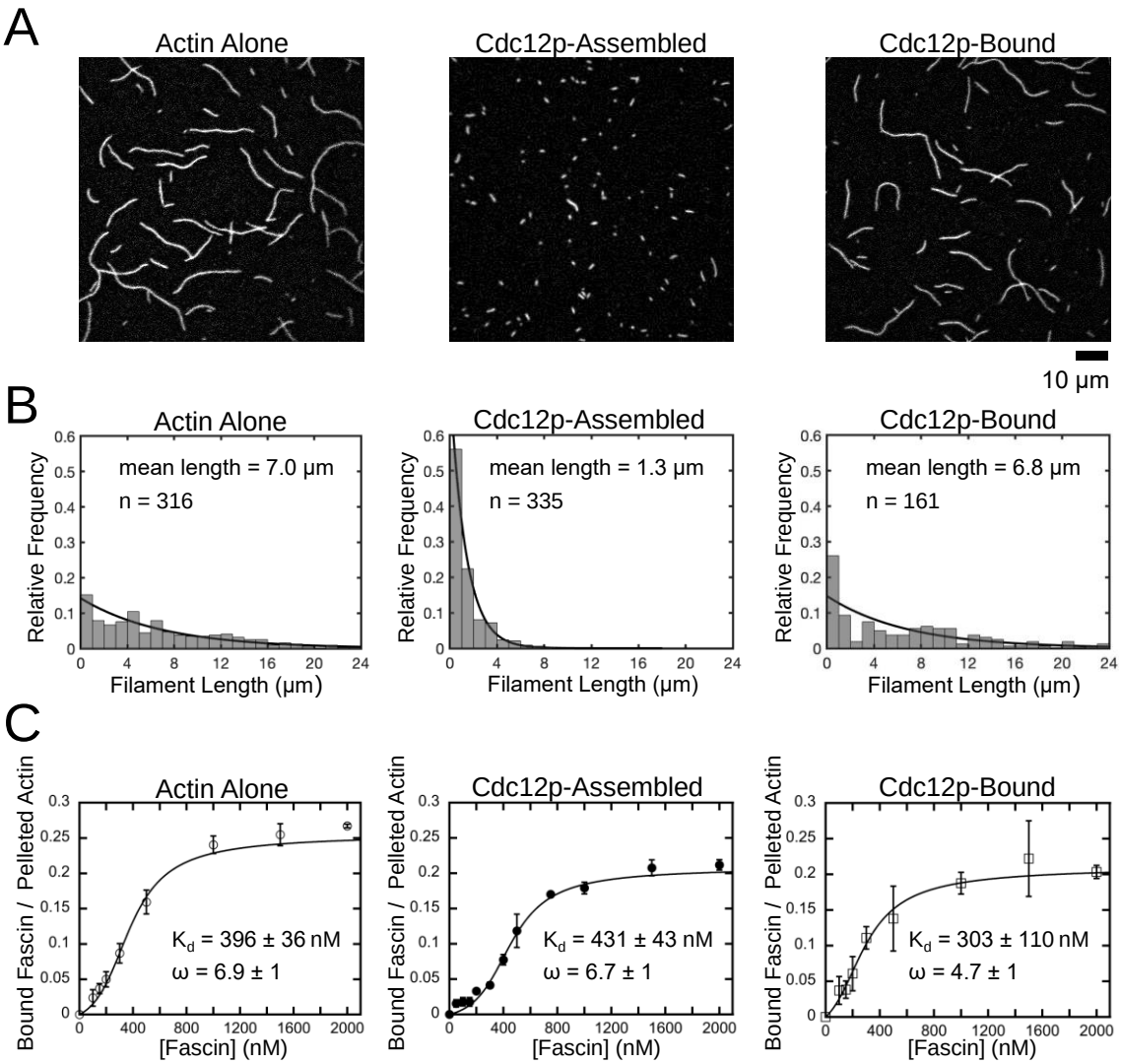

Figure 15. Fascin binds with similar affinity to short and long filaments. (A) Representative micrographs of filaments polymerized from 2 µM actin monomers in the absence or presence of 250 nM Cdc12p. Filaments were labeled with FITC-phalloidin, diluted in imaging buffer and visualized by TIRF microscopy. Cdc12p was added prior to polymerization in the "Cdc12p-Assembled" sample and post-polymerization in the "Cdc12p-Bound" sample. **(B)** Histograms of filament lengths measured at equilibrium for reactions polymerized in different conditions. The lines are exponential fits to the data. **(C)** Co-sedimentation assays measuring fascin binding to actin bundles assembled from

short and long filaments. Filaments were assembled in the absence or presence of Cdc12p and incubated with a range of fascin concentrations. Reactions were spun at low-speed (10,000 x *g* or 20,000 x *g* for long and short filaments, respectively) to pellet bundles and analyzed by SDS-PAGE. The intensity of the fascin band in the pelleted fraction was divided by the intensity of the actin band in the pelleted (i.e. bundled) fraction for each reaction. Lines are fits of the McGhee-von Hippel cooperative binding model, which yields a binding affinity (K_d) and cooperativity constant (ω). Error bars are the standard error of the mean values obtained from at least three independent replicates.

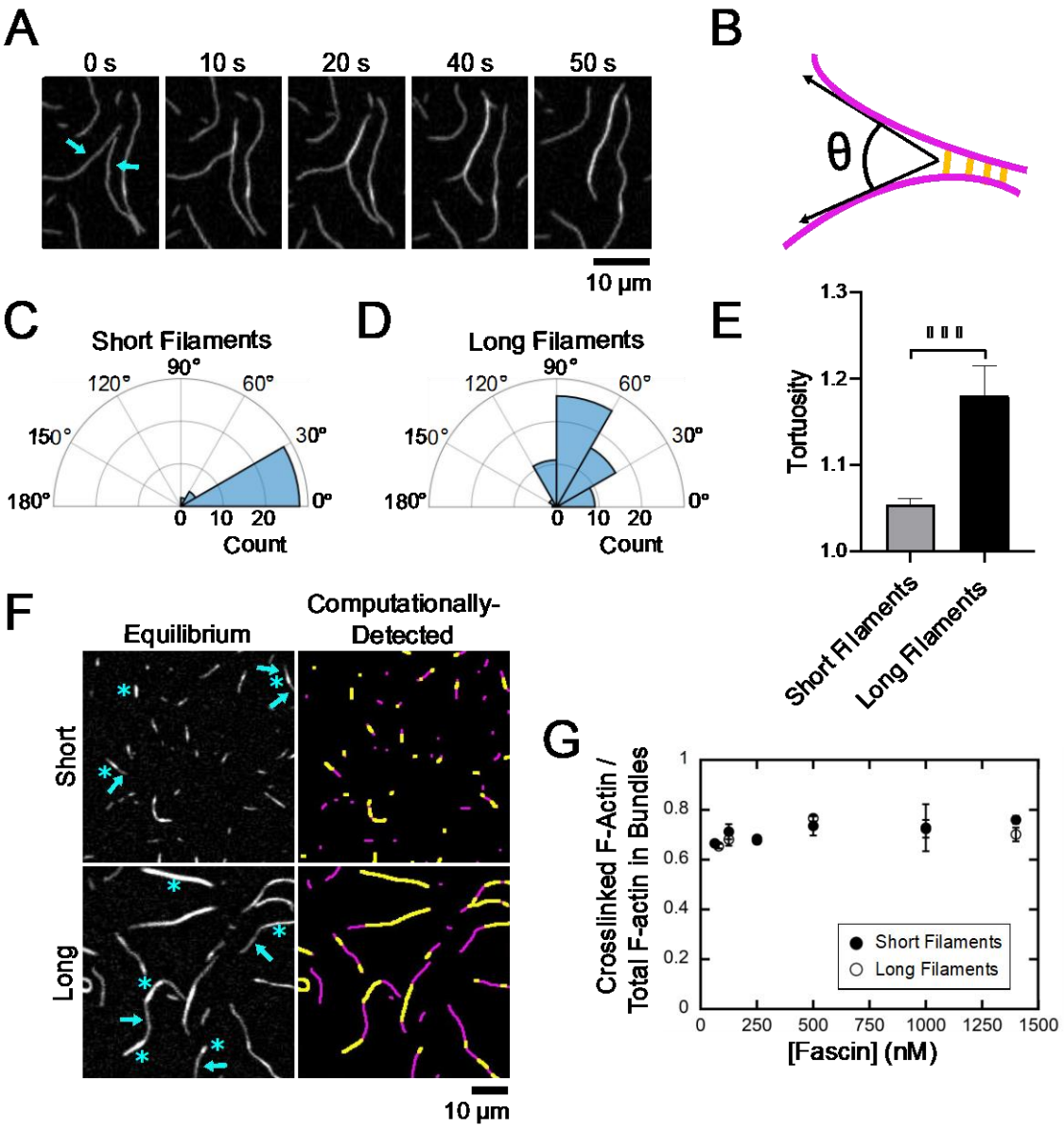

Figure 16. Fascin bundles short and long filaments cooperatively. Filaments were assembled by Cdc12p (short filaments) or through spontaneous actin polymerization (long filaments), labeled with FITC-phalloidin and imaged in microscopy buffer by TIRF microscopy following introduction of fascin. **(A)** Representative time series of TIRF micrographs showing bundling of two filaments in the presence of 1 µM fascin. **(B)** Schematic depicting the angle of alignment (θ) defined by two filaments (magenta) as they undergo bundling by fascin (yellow). **(C, D)** Polar histograms of angles of alignment

for short **(C)** and long filaments **(D)** during the formation of new bundles. Angle measurements were obtained for at least 30 bundling events from three independent replicates. **(E)** Tortuosity (ratio of contour length to end-to-end distance) of actin bundles assembled from short and long filaments ($n \geq 40$ bundles from at least three independent replicates). Statistical significance was established using Welch's t-test (***$p < 0.001$). **(F)** Micrographs of bundles of short and long actin filaments at equilibrium. Bundles contain crosslinked regions (blue asterisks in left panels, yellow stretches in right panels) and un-crosslinked regions (blue arrows in left panels, magenta stretches in right panels). **(G)** Dependence of the ratio of the crosslinked regions to the total filamentous actin contained in bundles on the concentration of fascin for short (closed circles) and long (open circles) filaments. Error bars are the standard error of the mean from at least three independent experiments.

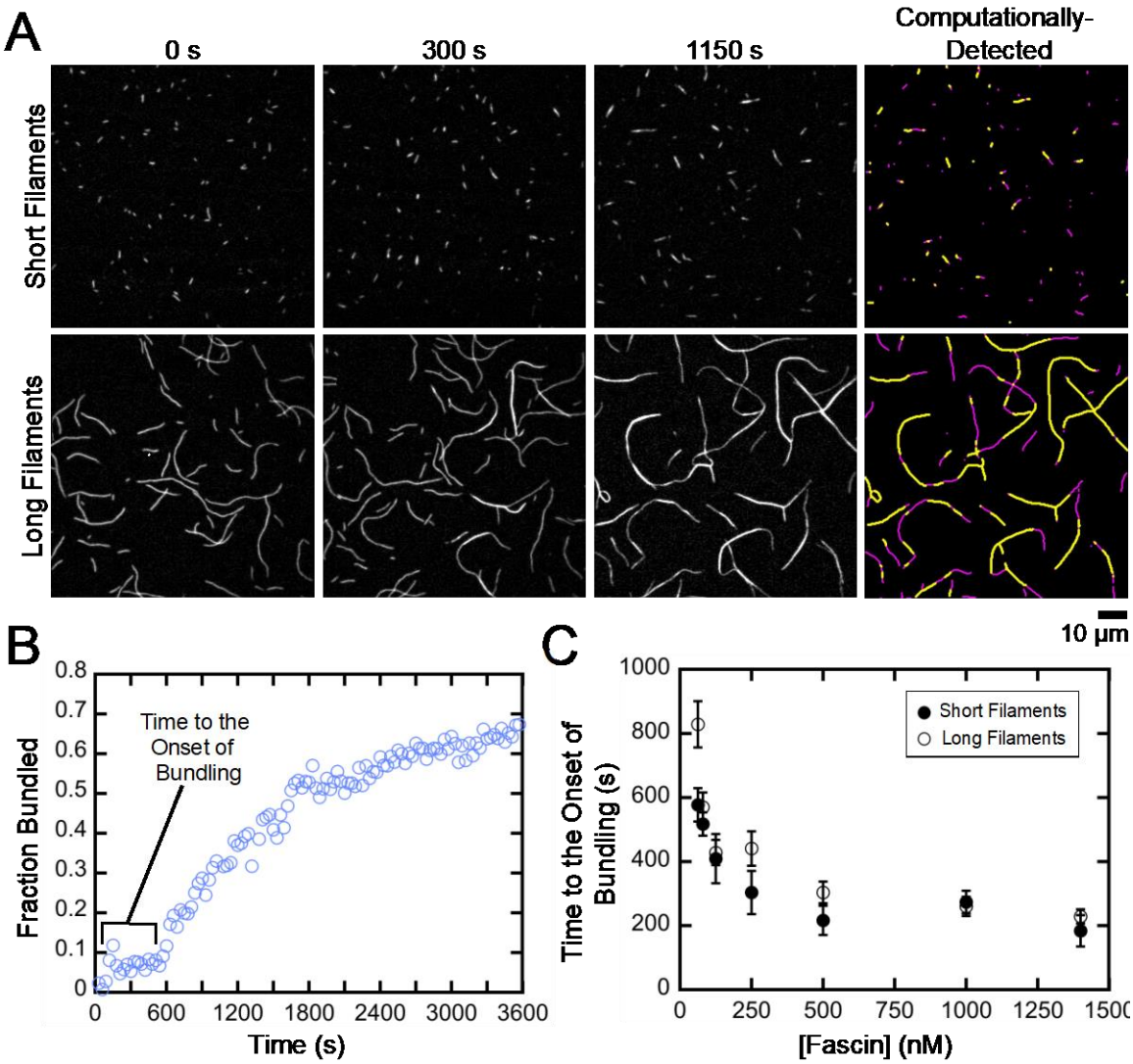

Figure 17. **A delay prior to the onset of fascin-mediated bundling is insensitive to filament length**. Filaments were assembled in the absence or presence of Cdc12p, labeled with FITC-phalloidin and visualized by TIRF microscopy following the addition of a range of concentrations of fascin. **(A)** Micrographs collected at various time points to show the progress of representative bundling reactions containing 1400 nM fascin. Panels on the right show automated detection of bundled (yellow) and single filament (magenta) stretches at 1150 s. **(B)** The fraction of the filamentous actin that is bundled over time for a representative reaction containing long filaments and 80 nM fascin. **(C)** Dependence of the length of the delay prior to the onset of bundling on the concentration

of fascin for reactions containing short (closed circles) and long (open circles) filaments. Error bars are the standard error of the mean of three independent replicates.

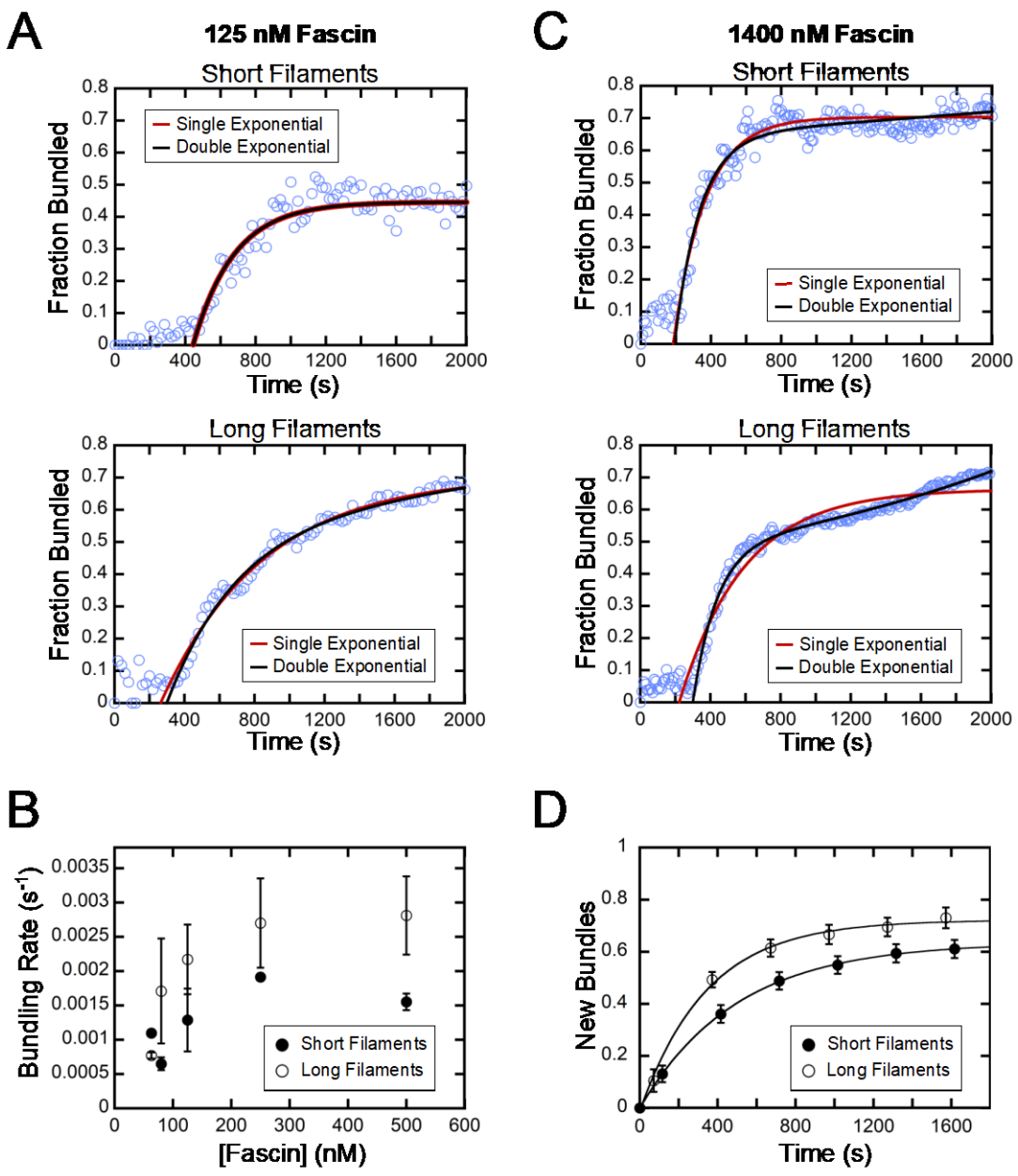

Figure 18. Fascin-mediated bundling occurs via distinct phases. A range of concentrations of fascin was introduced into reactions containing FITC-phalloidin-labeled actin filaments. **(A)** The fraction of the filamentous actin that is bundled over time in representative reactions containing 125 nM fascin. Red and black lines are single and double exponential fits to the data. **(B)** Bundling rates for short (closed circles) and long (open circles) actin filaments obtained from single exponential fits to bundling profiles

collected at sub-saturating fascin concentrations. **(C)** The fraction of the filamentous actin that is bundled over time in representative reactions containing 1400 nM fascin. Red and black lines are single and double exponential fits to the data. **(D)** The number of new bundles assembled from short (closed circles) and long filaments (open circles) over time in the presence of 1400 nM fascin. Lines are single exponential fits to the data. The number of bundles was normalized to the number of filaments present at the beginning of each reaction. Error bars are the standard error of the mean number of bundles measured in at least three independent replicates.

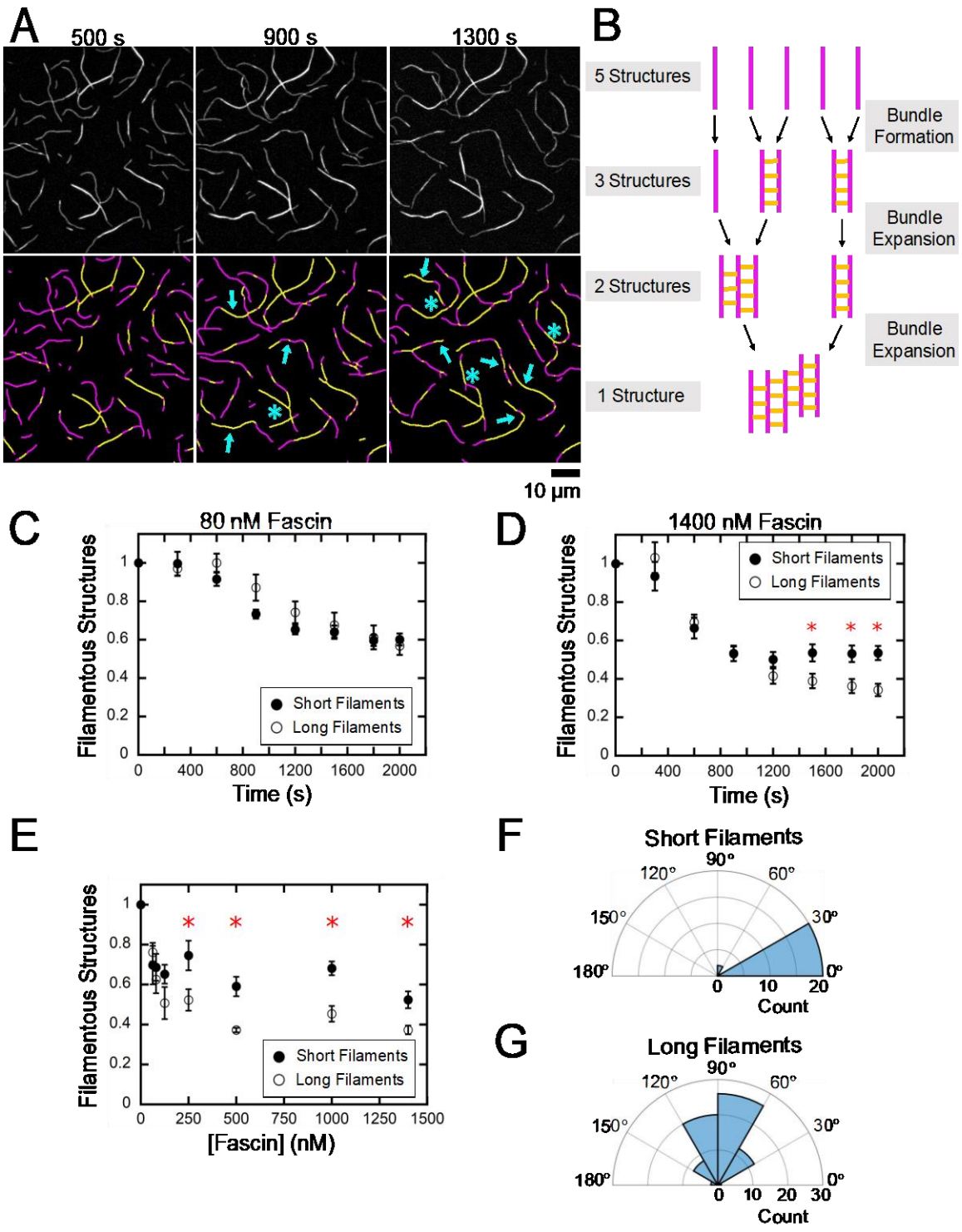

Figure 19. An increase in filament length promotes bundle expansion. Actin filaments were labeled by FITC-phalloidin, bundled by varying concentrations of fascin and imaged by TIRF microscopy. **(A)** *Top row,* TIRF Micrographs collected at 400 s

intervals spanning the first and second phases of a representative bundling reaction containing long filaments and 1400 nM fascin. *Bottom row,* Computationally-detected crosslinked (yellow*)* and un-crosslinked *(*magenta) actin filament stretches. Blue arrows indicate regions where bundle expansion has occurred. Blue asterisks indicate nonlinear bundle morphologies. **(B)** Schematic illustrating the relationship between bundle assembly progression and the number of filamentous structures contained in a bundling reaction. Filaments are depicted in magenta. Fascin-mediated crosslinks are shown in yellow. **(C-E)** The number of filamentous structures (i.e., the sum of the individual filaments and bundles) visualized per 6,400 μm^2 over time for reactions containing 80 nM **(C)** and 1400 nM **(D)** fascin. The number of bundles was normalized to the number of filaments present at the beginning of each reaction. Red asterisks indicate statistically significant differences ($p < 0.05$ using Welch's t-test) between measurements obtained for reactions containing short and long filaments. Error bars are the standard error of the mean number of filamentous structures measured in at least three independent replicates. **(E)** The dependence of the number of filamentous structures visualized in bundling reactions that have reached equilibrium on the concentration of fascin. **(F, G)** Polar histograms of angles of alignment for short **(F)** and long filaments **(G)** across three independent replicates.

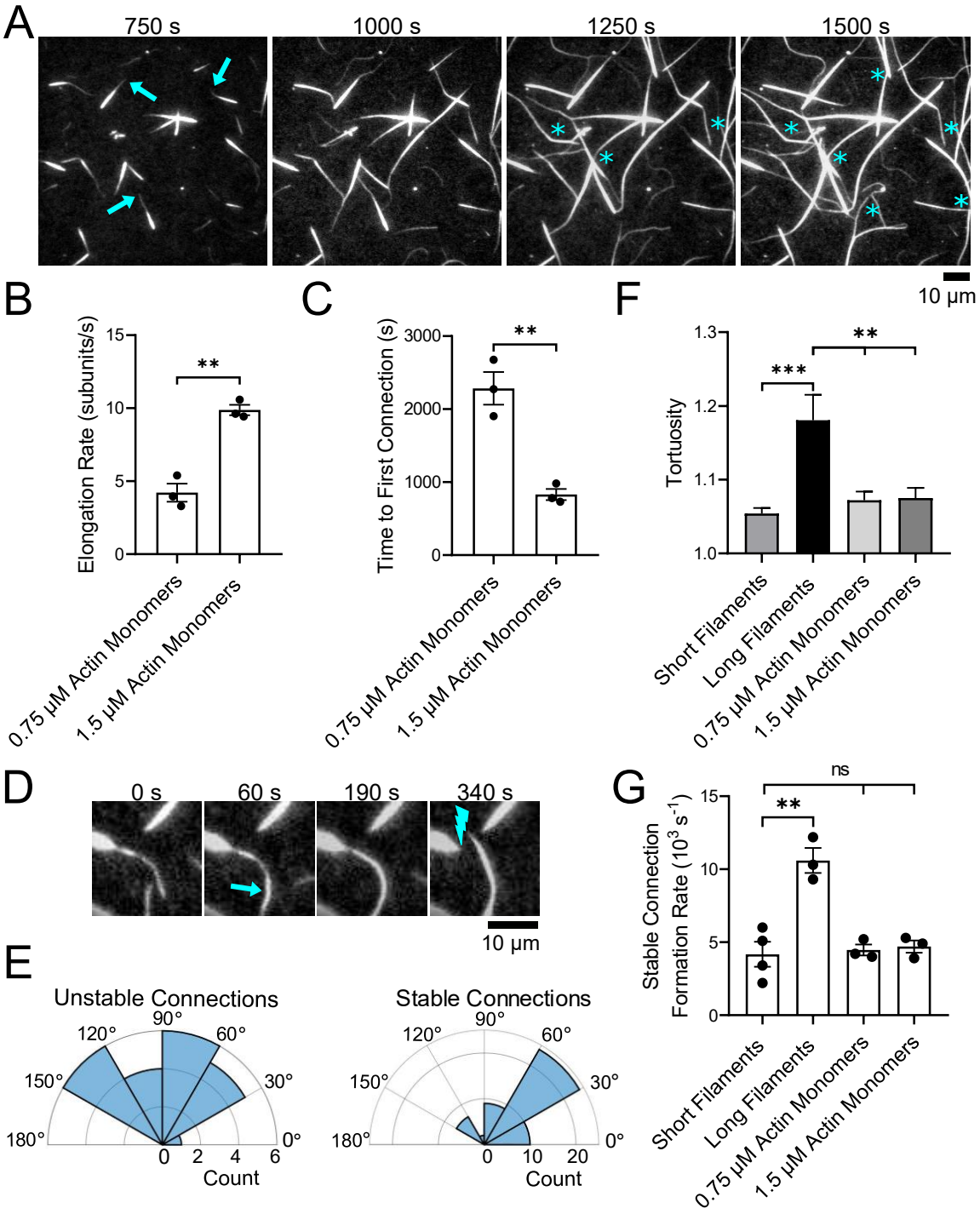

Figure 20. Bundles of short filaments remain discrete while elongating. Filaments were assembled in the presence of Cdc12p, labeled with FITC-phalloidin and bundled by 1 µM fascin. Bundles were visualized by TIRF microscopy following the introduction of 0.75 or 1.5 µM actin monomers, 10 µM *S. pombe* profilin, and 1 µM additional fascin. **(A)**

Time series of micrographs of preassembled bundles elongating following the addition of 1.5 μM actin monomers. Arrows indicate growing barbed ends. Blue asterisks denote crosslinking events that connect two pre-existing bundles. **(B)** Rates of bundle elongation. (**C)** Length of time required to form the first connection between bundles following the onset of elongation. **(D)** Micrographs depicting an example of two elongating bundles forming a short-lived connection. The arrow indicates the newly crosslinked region. The lightning bolt indicates the site of subsequent bundle breakage. **(E)** Polar histograms of angles of alignments for unstable (left) and stable (right) connections formed between preassembled bundles elongating in the presence of 1.5 μM actin monomers. **(F)** Tortuosity (ratio of bundle length to bundle end-to-end distance) of elongating actin bundles ($n \geq 40$ bundles from at least three independent replicates). **(G)** Rates at which stable connections are formed in reactions containing elongating bundles or filaments of constant length. In all graphs, asterisks indicate statistical significance (**$p < 0.01$). Black dots represent values from individual replicates. Error bars are the standard error of the mean measurements obtained from three independent experiments.

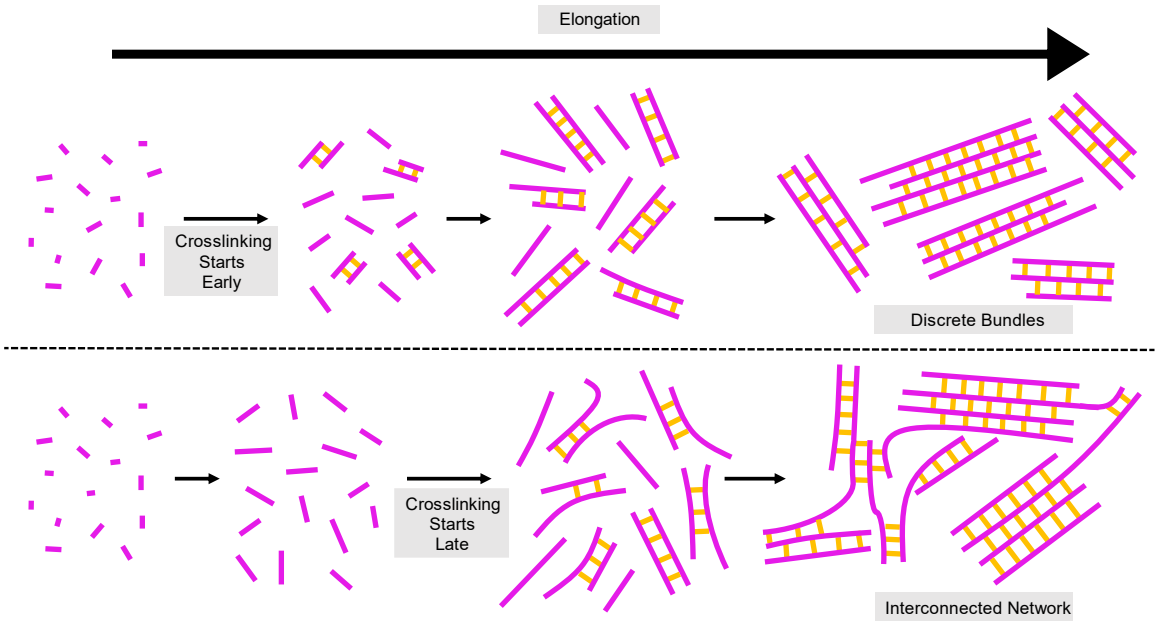

Figure 21. Assembly of crosslinked actin structures from elongating filaments. Proposed model for the role of filament length in the assembly of actin bundles. Elongating actin filaments and fascin-mediated crosslinks are depicted in magenta and yellow. Initiation of filament bundling early in elongation (when filaments are short) promotes the assembly of discrete bundles (top). Bundling at later stages of elongation (when filaments are longer) produces interconnected networks with irregular bundle morphologies (bottom).

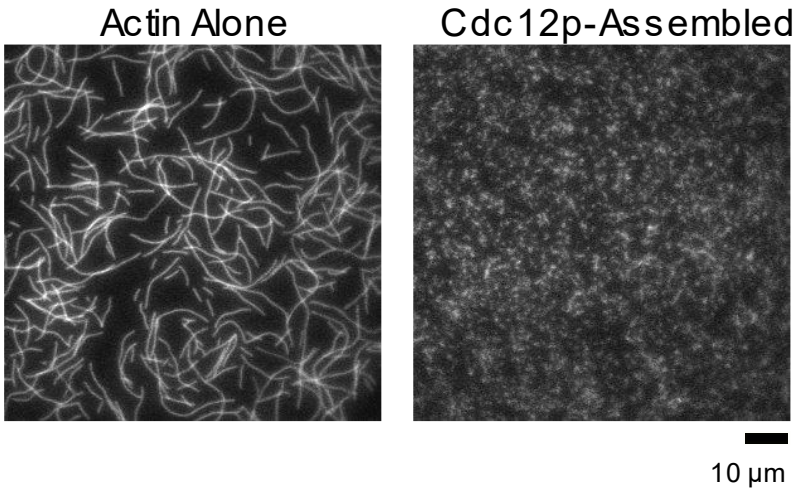

Supplementary Figure S1. Cdc12p increases the number of actin filaments assembled during polymerization reactions. 3 µM actin monomers were polymerized in the absence (left) or presence (right) of 750 nM Cdc12p, labeled with FITC-phalloidin, and visualized by TIRF microscopy.

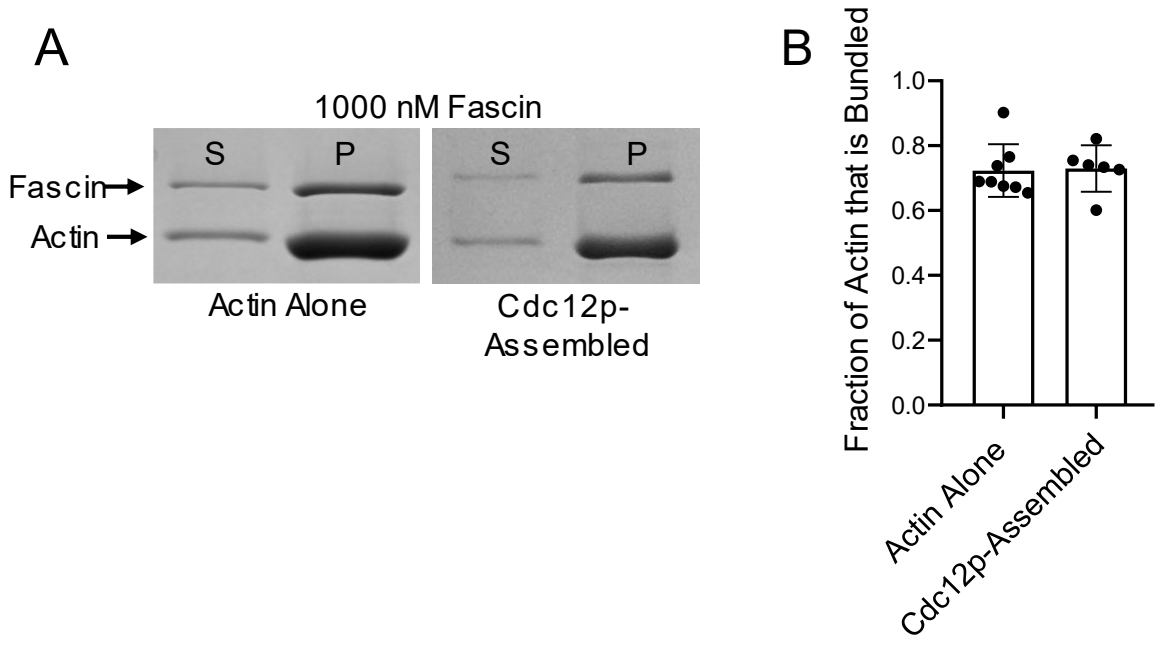

Supplementary Figure S2. Fascin efficiently bundles actin filaments with free and Cdc12p-bound barbed ends. Co-sedimentation assays measuring fascin-mediated bundling of actin filaments. Filaments were assembled from 2 µM actin monomers in the absence or presence of 250 nM Cdc12p and incubated with 1 µM fascin for 30 min at room temperature. Reactions were spun at low speed (10,000 x g or 20,000 x g for long and short filaments) to pellet bundles. **(A)** Representative SDS-PAGE gels showing the supernatant (S) and pellet (P) from reactions containing spontaneously- (left) and Cdc12p-assembled (right) actin filaments. **(B)** Quantification of the fraction of actin in each reaction that sediments into the pellet and is therefore bundled. Error bars are the standard deviation of values obtained from at least three independent replicates.

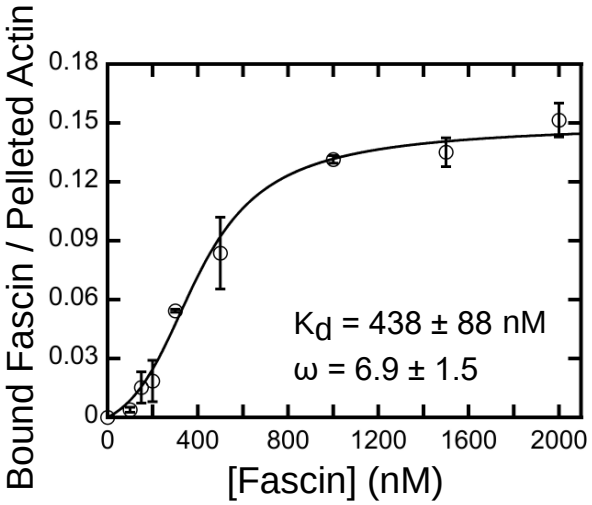

Supplementary Figure S3. Fascin-mediated bundling is insensitive to phalloidin labeling. Co-sedimentation assays measuring binding of a range of fascin concentrations to 2 µM FITC-phalloidin-labeled actin filaments. Reactions were spun at low speed (10,000 x g) to pellet bundles and analyzed by SDS-PAGE. The intensity of the pelleted fascin band was divided by the intensity of the pelleted (i.e., bundled) actin band in each reaction. Line is a fit of the McGhee-von Hippel cooperative binding model, which yields the binding affinity (K_d) and cooperativity constant (ω). Error bars are the standard error of the mean values obtained from at least three independent replicates.

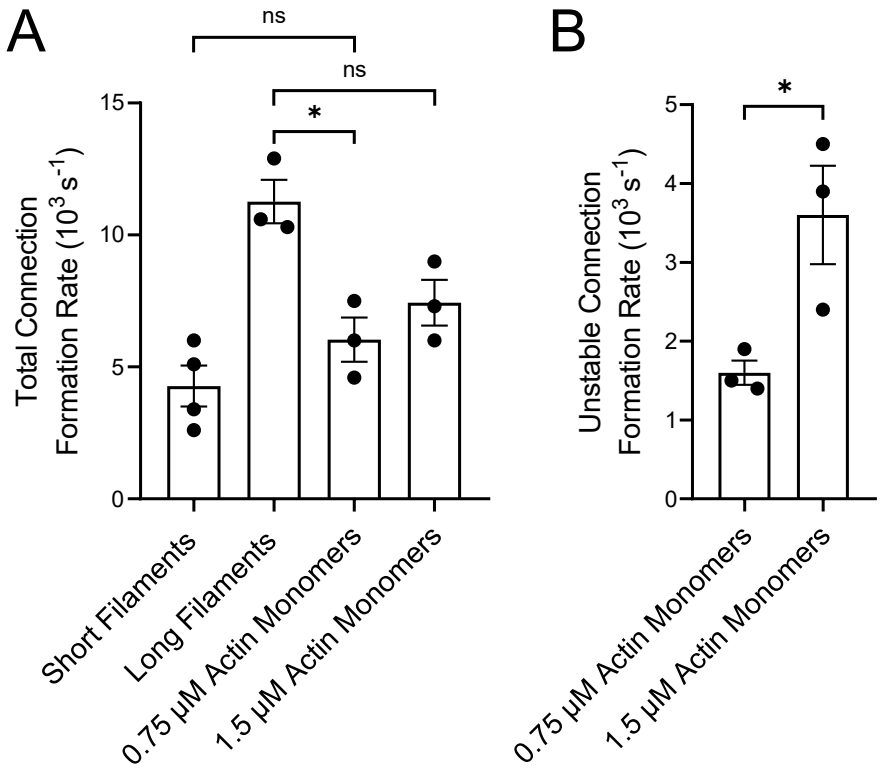

Supplementary Figure S4. Inter-bundle connections form at rates that depend on elongation rate. Filaments were assembled by Cdc12p (short filaments) or through spontaneous actin polymerization (long filaments), labeled with FITC-phalloidin and imaged in microscopy buffer by TIRF microscopy following introduction of fascin. Preassembled bundles were formed by incubating short filaments with 1 µM fascin prior to the introduction of 0.75 or 1.5 µM actin monomers, 10 µM *S. pombe* profilin, and 1 µM additional fascin. Error bars are the standard error of the mean rates measured from at least three independent replicates. **(A)** Rates at which inter-bundle connections are formed in reactions containing elongating bundles or filaments of constant length. Rates include both short-lived connections that break as elongation and crosslinking progress and stable connections that persist without breaking over the course of the reaction. **(B)** Rates at which unstable connections are formed in reactions containing elongating bundles.

FUTURE DIRECTIONS

In this thesis, I investigated the interdependence of actin filament nucleation, elongation, and crosslinking during actin structure assembly. I first explored the quantitative balance between formin-mediated nucleation and elongation, finding that nucleation by formins limits the influence of elongation on filament lengths. Next, I used these insights on filament length regulation to explore how elongation influences fascin-mediated bundling. The data show that crosslinking early in elongation (when filaments are short) hinders the formation of interconnected actin networks, thus suggesting that uncoordinated filament elongation and crosslinking can alter the architecture of bundled actin structures.

These key findings set up future inquiries into actin structure assembly, especially when combined with the microscopy assays and computational tools I developed. These inquiries should focus on resolving how different crosslinkers affect the role of elongation in crosslinked structure assembly. In my work, I found that fascin deters the formation of stable connections between elongating bundles, but it is still unclear whether flexible crosslinkers like alpha-actinin and filamin A behave differently and allow more inter-bundle connections to form. This would make actin structures crosslinked by alpha-actinin or filamin A much more sensitive to changes in filament length than structures crosslinked by fascin.

Another area of inquiry requiring further attention is the interplay between nucleation, elongation, and crosslinking in cellular environments. To dissect the relationship between formin-mediated nucleation and elongation in cells, a useful line of investigation involves uncoupling formin's nucleation and elongation activities and observing the subsequent effects on crosslinked actin structures. Fortunately, a previous study suggests that uncoupling these activities is relatively straightforward and easily

achieved; mutating specific Bni1p residues involved in salt bridge formation significantly decreases the nucleation efficiency of Bni1p but does not affect its elongation properties (Baker et al., 2015). My *in vitro* work on actin filament assembly provides a mechanistic foundation upon which these future studies can build.

Precise modulation of formin activity can also inform our understanding of elongation and crosslinking in cellular environments. Previous work in the Courtemanche lab has shown that replacing polyproline tracts in formin FH1 domains with polyglycine-serine sequences (which cannot bind profilin) alters formin-mediated elongation rates (Zweifel and Courtemanche, 2020). These mutations are not likely to affect formin's nucleation activity or regulation by Rho GTPases, so expressing these mutants and analyzing the resulting phenotypes would allow us to specifically probe the consequences of tuning actin elongation rates. More broadly, this strategy of finetuning formin activity in cells may also shed light on how different isoforms are tailored to their cellular roles.

Although many open questions remain, the studies described in this thesis offer important insight into the interdependence of nucleation, elongation, and crosslinking and provide a useful framework for future investigations into the assembly of specialized actin structures.

REFERENCES

Ahuja, R., Pinyol, R., Reichenbach, N., Custer, L., Klingensmith, J., Kessels, M. M., et al. (2007). Cordon-Bleu Is an Actin Nucleation Factor and Controls Neuronal Morphology. *Cell* 131, 337–350. doi: 10.1016/j.cell.2007.08.030.

Ajeti, V., Tabatabai, A. P., Fleszar, A. J., Staddon, M. F., Seara, D. S., Suarez, C., et al. (2019). Wound Healing Coordinates Actin Architectures to Regulate Mechanical Work. *Nat. Phys.* 15, 696. doi: 10.1038/s41567-019-0485-9.

Alizadeh, A. M., Shiri, S., and Farsinejad, S. (2014). Metastasis review: from bench to bedside. *Tumor Biol.* 35, 8483–8523. doi: 10.1007/s13277-014-2421-z.

Arjonen, A., Kaukonen, R., and Ivaska, J. (2011). Filopodia and adhesion in cancer cell motility. *Cell Adh Migr* 5, 421–430. doi: 10.4161/cam.5.5.17723.

Arthur, A. L., Crawford, A., Houdusse, A., and Titus, M. A. (2021). VASP-mediated actin dynamics activate and recruit a filopodia myosin. *eLife* 10, e68082. doi: 10.7554/eLife.68082.

Aydin, F., Courtemanche, N., Pollard, T. D., and Voth, G. A. (2018). Gating mechanisms during actin filament elongation by formins. *eLife* 7, e37342. doi: 10.7554/eLife.37342.

Baker, J. L., Courtemanche, N., Parton, D. L., McCullagh, M., Pollard, T. D., and Voth, G. A. (2015). Electrostatic Interactions Between the Bni1p Formin FH2 Domain and Actin Influence Actin Filament Nucleation. *Structure* 23, 68–79. doi: 10.1016/j.str.2014.10.014.

Bartles, J. R. (2000). Parallel actin bundles and their multiple actin-bundling proteins. *Current Opinion in Cell Biology* 12, 72–78. doi: 10.1016/S0955-0674(99)00059-9.

Baviskar, S. N. (2011). A Quick & Automated Method for Measuring Cell Area using ImageJ. *ambt* 73, 554–556. doi: 10.1525/abt.2011.73.9.9.

Blanchoin, L., Boujemaa-Paterski, R., Sykes, C., and Plastino, J. (2014). Actin Dynamics, Architecture, and Mechanics in Cell Motility. *Physiological Reviews* 94, 235–263. doi: 10.1152/physrev.00018.2013.

Breitsprecher, D., Jaiswal, R., Bombardier, J. P., Gould, C. J., Gelles, J., and Goode, B. L. (2012). Rocket launcher mechanism of collaborative actin assembly defined by single-molecule imaging. *Science* 336, 1164–1168. doi: 10.1126/science.1218062.

Breitsprecher, D., Kiesewetter, A. K., Linkner, J., Urbanke, C., Resch, G. P., Small, J. V., et al. (2008). Clustering of VASP actively drives processive, WH2 domain-mediated actin filament elongation. *EMBO J* 27, 2943–2954. doi: 10.1038/emboj.2008.211.

Breitsprecher, D., Koestler, S. A., Chizhov, I., Nemethova, M., Mueller, J., Goode, B. L., et al. (2011). Cofilin cooperates with fascin to disassemble filopodial actin filaments. *Journal of Cell Science* 124, 3305–3318. doi: 10.1242/jcs.086934.

Bryan, J., and Kane, R. E. (1978). Separation and interaction of the major components of sea urchin actin gel. *Journal of Molecular Biology* 125, 207–224. doi: 10.1016/0022-2836(78)90345-5.

Bugyi, B., and Kellermayer, M. (2020). The discovery of actin: “to see what everyone else has seen, and to think what nobody has thought”. *J Muscle Res Cell Motil* 41, 3–9. doi: 10.1007/s10974-019-09515-z.

Bugyi, B., Papp, G., Hild, G., Lõrinczy, D., Nevalainen, E. M., Lappalainen, P., et al. (2006). Formins regulate actin filament flexibility through long range allosteric interactions. *J Biol Chem* 281, 10727–10736. doi: 10.1074/jbc.M510252200.

Buttery, S. M., Yoshida, S., and Pellman, D. (2007). Yeast Formins Bni1 and Bnr1 Utilize Different Modes of Cortical Interaction during the Assembly of Actin Cables. *MBoC* 18, 1826–1838. doi: 10.1091/mbc.e06-09-0820.

Chalkia, D., Nikolaidis, N., Makalowski, W., Klein, J., and Nei, M. (2008). Origins and Evolution of the Formin Multigene Family That Is Involved in the Formation of Actin Filaments. *Molecular Biology and Evolution* 25, 2717–2733. doi: 10.1093/molbev/msn215.

Chang, F., Drubin, D., and Nurse, P. (1997). cdc12p, a Protein Required for Cytokinesis in Fission Yeast, Is a Component of the Cell Division Ring and Interacts with Profilin. *J Cell Biol* 137, 169–182.

Chen, Q., and Pollard, T. D. (2011). Actin filament severing by cofilin is more important for assembly than constriction of the cytokinetic contractile ring. *Journal of Cell Biology* 195, 485–498. doi: 10.1083/jcb.201103067.

Chesarone-Cataldo, M., Guérin, C., Yu, J. H., Wedlich-Soldner, R., Blanchoin, L., and Goode, B. L. (2011). The myosin passenger protein Smy1 controls actin cable structure and dynamics by acting as a formin damper. *Dev Cell* 21, 217–230. doi: 10.1016/j.devcel.2011.07.004.

Chugh, P., Clark, A. G., Smith, M. B., Cassani, D. A. D., Dierkes, K., Ragab, A., et al. (2017). Actin cortex architecture regulates cell surface tension. *Nat Cell Biol* 19, 689–697. doi: 10.1038/ncb3525.

Chugh, P., and Paluch, E. K. (2018). The actin cortex at a glance. *Journal of Cell Science* 131, jcs186254. doi: 10.1242/jcs.186254.

Claessens, M. M. A. E., Bathe, M., Frey, E., and Bausch, A. R. (2006). Actin-binding proteins sensitively mediate F-actin bundle stiffness. *Nature Mater* 5, 748–753. doi: 10.1038/nmat1718.

Cooper, J. A., Buhle, E. L., Walker, S. B., Tsong, T. Y., and Pollard, T. D. (1983). Kinetic evidence for a monomer activation step in actin polymerization. *Biochemistry* 22, 2193–2202. doi: 10.1021/bi00278a021.

Courson, D. S., and Rock, R. S. (2010). Actin Cross-link Assembly and Disassembly Mechanics for α-Actinin and Fascin*. *Journal of Biological Chemistry* 285, 26350–26357. doi: 10.1074/jbc.M110.123117.

Courtemanche, N. (2018). Mechanisms of formin-mediated actin assembly and dynamics. *Biophys Rev* 10, 1553–1569. doi: 10.1007/s12551-018-0468-6.

Courtemanche, N., and Pollard, T. D. (2013). Interaction of profilin with the barbed end of actin filaments. *Biochemistry* 52, 6456–6466. doi: 10.1021/bi400682n.

De La Cruz, E. M. (2005). Cofilin Binding to Muscle and Non-muscle Actin Filaments: Isoform-dependent Cooperative Interactions. *Journal of Molecular Biology* 346, 557–564. doi: 10.1016/j.jmb.2004.11.065.

Dominguez, R., and Holmes, K. C. (2011). Actin Structure and Function. *Annual Review of Biophysics* 40, 169–186. doi: 10.1146/annurev-biophys-042910-155359.

Dutta, P., Das, S., and Maiti, S. (2017). Non diaphanous formin delphilin acts as a barbed end capping protein. *Experimental Cell Research* 357, 163–169. doi: 10.1016/j.yexcr.2017.05.014.

Ennomani, H., Letort, G., Guerin, C., Martiel, J.-L., Cao, W., Nedelec, F., et al. (2016). Architecture and Connectivity Govern Actin Network Contractility. *Curr. Biol.* 26, 616–626. doi: 10.1016/j.cub.2015.12.069.

Esue, O., Harris, E. S., Higgs, H. N., and Wirtz, D. (2008). The Filamentous Actin Cross-Linking/Bundling Activity of Mammalian Formins. *Journal of molecular biology* 384, 324–334. doi: 10.1016/j.jmb.2008.09.043.

Falzone, T. T., Lenz, M., Kovar, D. R., and Gardel, M. L. (2012). Assembly kinetics determine the architecture of α-actinin crosslinked F-actin networks. *Nat Commun* 3, 861. doi: 10.1038/ncomms1862.

Falzone, T. T., Oakes, P. W., Sees, J., Kovar, D. R., and Gardel, M. L. (2013). Actin Assembly Factors Regulate the Gelation Kinetics and Architecture of F-actin Networks. *Biophysical Journal* 104, 1709–1719. doi: 10.1016/j.bpj.2013.01.017.

Feierbach, B., and Chang, F. (2001). Roles of the fission yeast formin for3p in cell polarity, actin cable formation and symmetric cell division. *Current Biology* 11, 1656–1665. doi: 10.1016/S0960-9822(01)00525-5.

Feng, D., DuMontier, C., and Pollak, M. R. (2015). The role of alpha-actinin-4 in human kidney disease. *Cell & Bioscience* 5, 44. doi: 10.1186/s13578-015-0036-8.

Flanagan, L. A., Chou, J., Falet, H., Neujahr, R., Hartwig, J. H., and Stossel, T. P. (2001). Filamin A, the Arp2/3 complex, and the morphology and function of cortical actin filaments in human melanoma cells. *J Cell Biol* 155, 511–518. doi: 10.1083/jcb.200105148.

Fujiwara, K., Porter, M. E., and Pollard, T. D. (1978). Alpha-actinin localization in the cleavage furrow during cytokinesis. *J Cell Biol* 79, 268–275. doi: 10.1083/jcb.79.1.268.

Goh, W. I., Sudhaharan, T., Lim, K. B., Sem, K. P., Lau, C. L., and Ahmed, S. (2011). Rif-mDia1 Interaction Is Involved in Filopodium Formation Independent of Cdc42 and Rac Effectors. *Journal of Biological Chemistry* 286, 13681–13694. doi: 10.1074/jbc.M110.182683.

Gordon-Alonso, M., Veiga, E., and Sanchez-Madrid, F. (2010). Actin dynamics at the immunological synapse. *Cell Health Cytoskelet.* 2, 33–47.

Gressin, L., Guillotin, A., Guerin, C., Blanchoin, L., and Michelot, A. (2015). Architecture Dependence of Actin Filament Network Disassembly. *Curr. Biol.* 25, 1437–1447. doi: 10.1016/j.cub.2015.04.011.

Grishagin, I. V. (2015). Automatic cell counting with ImageJ. *Anal Biochem* 473, 63–65. doi: 10.1016/j.ab.2014.12.007.

Gupton, S. L., Eisenmann, K., Alberts, A. S., and Waterman-Storer, C. M. (2007). mDia2 regulates actin and focal adhesion dynamics and organization in the lamella for efficient epithelial cell migration. *Journal of Cell Science* 120, 3475–3487. doi: 10.1242/jcs.006049.

Hampton, C. M., Taylor, D. W., and Taylor, K. A. (2007). Novel Structures for α-Actinin:F-Actin Interactions and their Implications for Actin–Membrane Attachment and Tension Sensing in the Cytoskeleton. *Journal of Molecular Biology* 368, 92–104. doi: 10.1016/j.jmb.2007.01.071.

Harris, A. R., Jreij, P., and Fletcher, D. A. (2018). Mechanotransduction by the Actin Cytoskeleton: Converting Mechanical Stimuli into Biochemical Signals. *Annual Review of Biophysics* 47, 617–631. doi: 10.1146/annurev-biophys-070816-033547.

Harris, E. S., Rouiller, I., Hanein, D., and Higgs, H. N. (2006). Mechanistic differences in actin bundling activity of two mammalian formins, FRL1 and mDia2. *J Biol Chem* 281, 14383–14392. doi: 10.1074/jbc.m510923200.

Hashimoto, Y., Kim, D. J., and Adams, J. C. (2011). The roles of fascins in health and disease. *The Journal of Pathology* 224, 289–300. doi: 10.1002/path.2894.

Hashimoto, Y., Skacel, M., and Adams, J. C. (2005). Roles of fascin in human carcinoma motility and signaling: Prospects for a novel biomarker? *The International Journal of Biochemistry & Cell Biology* 37, 1787–1804. doi: 10.1016/j.biocel.2005.05.004.

Higgs, H. N. (2005). Formin proteins: a domain-based approach. *Trends in Biochemical Sciences* 30, 342–353. doi: 10.1016/j.tibs.2005.04.014.

Higgs, H. N., and Peterson, K. J. (2005). Phylogenetic Analysis of the Formin Homology 2 Domain. *MBoC* 16, 1–13. doi: 10.1091/mbc.e04-07-0565.

Horan, B. G., Zerze, G. H., Kim, Y. C., Vavylonis, D., and Mittal, J. (2018). Computational modeling highlights the role of the disordered Formin Homology 1 domain in profilin-actin transfer. *FEBS Letters* 592, 1804–1816. doi: 10.1002/1873-3468.13088.

Isambert, H., Venier, P., Maggs, A. C., Fattoum, A., Kassab, R., Pantaloni, D., et al. (1995). Flexibility of Actin Filaments Derived from Thermal Fluctuations: EFFECT OF BOUND NUCLEOTIDE, PHALLOIDIN, AND MUSCLE REGULATORY PROTEINS. *Journal of Biological Chemistry* 270, 11437–11444. doi: 10.1074/jbc.270.19.11437.

Jacquemet, G., Hamidi, H., and Ivaska, J. (2015). Filopodia in cell adhesion, 3D migration and cancer cell invasion. *Current Opinion in Cell Biology* 36, 23–31. doi: 10.1016/j.ceb.2015.06.007.

Jaiswal, R., Breitsprecher, D., Collins, A., Corrêa, I. R., Xu, M.-Q., and Goode, B. L. (2013). The Formin Daam1 and Fascin Directly Collaborate to Promote Filopodia Formation. *Current Biology* 23, 1373–1379. doi: 10.1016/j.cub.2013.06.013.

Jansen, S., Collins, A., Yang, C., Rebowski, G., Svitkina, T., and Dominguez, R. (2011). Mechanism of Actin Filament Bundling by Fascin. *J Biol Chem* 286, 30087–30096. doi: 10.1074/jbc.M111.251439.

Jegou, A., and Romet-Lemonne, G. (2020). The many implications of actin filament helicity. *Seminars in Cell & Developmental Biology* 102, 65–72. doi: 10.1016/j.semcdb.2019.10.018.

Johnson, M., East, D. A., and Mulvihill, D. P. (2014). Formins Determine the Functional Properties of Actin Filaments in Yeast. *Current Biology* 24, 1525–1530. doi: 10.1016/j.cub.2014.05.034.

Kallikourdis, M., Viola, A., and Benvenuti, F. (2015). Human Immunodeficiencies Related to Defective APC/T Cell Interaction. *Frontiers in Immunology* 6. Available at: https://www.frontiersin.org/articles/10.3389/fimmu.2015.00433 [Accessed July 5, 2022].

Kapoor, P., Chen, M., Winkler, D. D., Luger, K., and Shen, X. (2013). Evidence for monomeric actin function in INO80 chromatin remodeling. *Nat. Struct. Mol. Biol.* 20, 426. doi: 10.1038/nsmb.2529.

Kothari, P., Schiffhauer, E. S., and Robinson, D. N. (2017). “Chapter 18 - Cytokinesis from nanometers to micrometers and microseconds to minutes,” in *Methods in Cell Biology* Cytokinesis., ed. A. Echard (Academic Press), 307–322. doi: 10.1016/bs.mcb.2016.03.038.

Kovac, B., Teo, J. L., Makela, T. P., and Vallenius, T. (2013). Assembly of non-contractile dorsal stress fibers requires alpha-actinin-1 and Rac1 in migrating and spreading cells. *J. Cell Sci.* 126, 263–273. doi: 10.1242/jcs.115063.

Kovar, D. R. (2006). Molecular details of formin-mediated actin assembly. *Current Opinion in Cell Biology* 18, 11–17. doi: 10.1016/j.ceb.2005.12.011.

Kovar, D. R., Harris, E. S., Mahaffy, R., Higgs, H. N., and Pollard, T. D. (2006). Control of the Assembly of ATP- and ADP-Actin by Formins and Profilin. *Cell* 124, 423–435. doi: 10.1016/j.cell.2005.11.038.

Kovar, D. R., Kuhn, J. R., Tichy, A. L., and Pollard, T. D. (2003). The fission yeast cytokinesis formin Cdc12p is a barbed end actin filament capping protein gated by profilin. *Journal of Cell Biology* 161, 875–887. doi: 10.1083/jcb.200211078.

Kovar, D. R., and Pollard, T. D. (2004). Insertional assembly of actin filament barbed ends in association with formins produces piconewton forces. *Proceedings of the National Academy of Sciences* 101, 14725–14730. doi: 10.1073/pnas.0405902101.

Kuhn, J. R., and Pollard, T. D. (2005). Real-Time Measurements of Actin Filament Polymerization by Total Internal Reflection Fluorescence Microscopy. *Biophysical Journal* 88, 1387–1402. doi: 10.1529/biophysj.104.047399.

Labat-de-Hoz, L., and Alonso, M. A. (2021). Formins in Human Disease. *Cells* 10, 2554. doi: 10.3390/cells10102554.

Lamb, M. C., and Tootle, T. L. (2020). Fascin in Cell Migration: More Than an Actin Bundling Protein. *Biology* 9, 403. doi: 10.3390/biology9110403.

Lambrechts, A., Gevaert, K., Cossart, P., Vandekerckhove, J., and Van Troys, M. (2008). Listeria comet tails: the actin-based motility machinery at work. *Trends in Cell Biology* 18, 220–227. doi: 10.1016/j.tcb.2008.03.001.

Laporte, D., Ojkic, N., Vavylonis, D., and Wu, J.-Q. (2012). α-Actinin and fimbrin cooperate with myosin II to organize actomyosin bundles during contractile-ring assembly. *Mol Biol Cell* 23, 3094–3110. doi: 10.1091/mbc.E12-02-0123.

Lappalainen, P. (2016). Actin-binding proteins: the long road to understanding the dynamic landscape of cellular actin networks. *Molecular biology of the cell* 27, 2519–2522.

Lei, W., Omotade, O. F., Myers, K. R., and Zheng, J. Q. (2016). Actin cytoskeleton in dendritic spine development and plasticity. *Curr. Opin. Neurobiol.* 39, 86–92. doi: 10.1016/j.conb.2016.04.010.

Li, A., Dawson, J. C., Forero-Vargas, M., Spence, H. J., Yu, X., König, I., et al. (2010). The Actin-Bundling Protein Fascin Stabilizes Actin in Invadopodia and Potentiates Protrusive Invasion. *Current Biology* 20, 339–345. doi: 10.1016/j.cub.2009.12.035.

Liu, H., Zhang, Y., Li, L., Cao, J., Guo, Y., Wu, Y., et al. (2021). Fascin actin-bundling protein 1 in human cancer: Promising biomarker or therapeutic target? *Mol. Ther.-Oncolytics* 20, 240–264. doi: 10.1016/j.omto.2020.12.014.

Lizárraga, F., Poincloux, R., Romao, M., Montagnac, G., Le Dez, G., Bonne, I., et al. (2009). Diaphanous-related formins are required for invadopodia formation and

invasion of breast tumor cells. *Cancer Res* 69, 2792–2800. doi: 10.1158/0008-5472.CAN-08-3709.

Lu, J., Meng, W., Poy, F., Maiti, S., Goode, B. L., and Eck, M. J. (2007). Structure of the FH2 Domain of Daam1: Implications for Formin Regulation of Actin Assembly. *Journal of Molecular Biology* 369, 1258–1269. doi: 10.1016/j.jmb.2007.04.002.

Ma, R., and Berro, J. (2018). Structural organization and energy storage in crosslinked actin assemblies. *PLOS Computational Biology* 14, e1006150. doi: 10.1371/journal.pcbi.1006150.

Mallavarapu, A., and Mitchison, T. (1999). Regulated Actin Cytoskeleton Assembly at Filopodium Tips Controls Their Extension and Retraction. *Journal of Cell Biology* 146, 1097–1106. doi: 10.1083/jcb.146.5.1097.

Martin, T. G., and Kirk, J. A. (2020). Under construction: the dynamic assembly, maintenance, and degradation of the cardiac sarcomere. *J Mol Cell Cardiol* 148, 89–102. doi: 10.1016/j.yjmcc.2020.08.018.

Mattila, P. K., and Lappalainen, P. (2008). Filopodia: molecular architecture and cellular functions. *Nat Rev Mol Cell Biol* 9, 446–454. doi: 10.1038/nrm2406.

McCullough, B. R., Blanchoin, L., Martiel, J.-L., and De La Cruz, E. M. (2008). Cofilin Increases the Bending Flexibility of Actin Filaments: Implications for Severing and Cell Mechanics. *Journal of Molecular Biology* 381, 550–558. doi: 10.1016/j.jmb.2008.05.055.

McGhee, J. D., and von Hippel, P. H. (1974). Theoretical aspects of DNA-protein interactions: co-operative and non-co-operative binding of large ligands to a one-dimensional homogeneous lattice. *J Mol Biol* 86, 469–489. doi: 10.1016/0022-2836(74)90031-x.

Mellor, H. (2010). The role of formins in filopodia formation. *Biochimica et Biophysica Acta (BBA) - Molecular Cell Research* 1803, 191–200. doi: 10.1016/j.bbamcr.2008.12.018.

Mersich, A. T., Miller, M. R., Chkourko, H., and Blystone, S. D. (2010). The Formin FRL1 (FMNL1) Is An Essential Component of Macrophage Podosomes. *Cytoskeleton (Hoboken, N.j.)* 67, 573. doi: 10.1002/cm.20468.

Miao, Y., Han, X., Zheng, L., Xie, Y., Mu, Y., Yates, J. R., et al. (2016). Fimbrin phosphorylation by metaphase Cdk1 regulates actin cable dynamics in budding yeast. *Nat Commun* 7, 11265. doi: 10.1038/ncomms11265.

Michelot, A., and Drubin, D. G. (2011). Building distinct actin filament networks in a common cytoplasm. *Curr Biol* 21, R560-569. doi: 10.1016/j.cub.2011.06.019.

Mizuno, H., Higashida, C., Yuan, Y., Ishizaki, T., Narumiya, S., and Watanabe, N. (2011). Rotational movement of the formin mDia1 along the double helical strand of an actin filament. *Science* 331, 80–83. doi: 10.1126/science.1197692.

Mizuno, H., Tanaka, K., Yamashiro, S., Narita, A., and Watanabe, N. (2018). Helical rotation of the diaphanous-related formin mDia1 generates actin filaments resistant to cofilin. *Proceedings of the National Academy of Sciences* 115, E5000–E5007. doi: 10.1073/pnas.1803415115.

Mooren, O. L., Galletta, B. J., and Cooper, J. A. (2012). Roles for Actin Assembly in Endocytosis. *Annual Review of Biochemistry* 81, 661–686. doi: 10.1146/annurev-biochem-060910-094416.

Moseley, J. B., and Goode, B. L. (2005). Differential Activities and Regulation of Saccharomyces cerevisiae Formin Proteins Bni1 and Bnr1 by Bud6 *. *Journal of Biological Chemistry* 280, 28023–28033. doi: 10.1074/jbc.M503094200.

Moseley, J. B., Sagot, I., Manning, A. L., Xu, Y., Eck, M. J., Pellman, D., et al. (2004). A Conserved Mechanism for Bni1- and mDia1-induced Actin Assembly and Dual Regulation of Bni1 by Bud6 and Profilin. *MBoC* 15, 896–907. doi: 10.1091/mbc.e03-08-0621.

Mukhina, S., Wang, Y.-L., and Murata-Hori, M. (2007). Alpha-actinin is required for tightly regulated remodeling of the actin cortical network during cytokinesis. *Dev Cell* 13, 554–565. doi: 10.1016/j.devcel.2007.08.003.

Murk, K., Ornaghi, M., and Schiweck, J. (2021). Profilin Isoforms in Health and Disease – All the Same but Different. *Frontiers in Cell and Developmental Biology* 9. Available at: https://www.frontiersin.org/article/10.3389/fcell.2021.681122 [Accessed March 28, 2022].

Murphy, A. C. H., Lindsay, A. J., McCaffrey, M. W., Djinovic-Carugo, K., and Young, P. W. (2016). Congenital macrothrombocytopenia-linked mutations in the actin-binding domain of alpha-actinin-1 enhance F-actin association. *FEBS Lett.* 590, 685–695. doi: 10.1002/1873-3468.12101.

Murphy, D. A., and Courtneidge, S. A. (2011). The “ins” and “outs” of podosomes and invadopodia: characteristics, formation and function. *Nat Rev Mol Cell Biol* 12, 413–426. doi: 10.1038/nrm3141.

Otomo, T., Tomchick, D. R., Otomo, C., Panchal, S. C., Machius, M., and Rosen, M. K. (2005). Structural basis of actin filament nucleation and processive capping by a formin homology 2 domain. *Nature* 433, 488–494. doi: 10.1038/nature03251.

Ozaki-Kuroda, K., Yamamoto, Y., Nohara, H., Kinoshita, M., Fujiwara, T., Irie, K., et al. (2001). Dynamic Localization and Function of Bni1p at the Sites of Directed Growth in Saccharomyces cerevisiae. *Molecular and Cellular Biology* 21, 827–839. doi: 10.1128/MCB.21.3.827-839.2001.

Panzer, L., Trübe, L., Klose, M., Joosten, B., Slotman, J., Cambi, A., et al. (2016). The formins FHOD1 and INF2 regulate inter- and intra-structural contractility of podosomes. *Journal of Cell Science* 129, 298–313. doi: 10.1242/jcs.177691.

Papp, G., Bugyi, B., Ujfalusi, Z., Barko, S., Hild, G., Somogyi, B., et al. (2006). Conformational changes in actin filaments induced by formin binding to the barbed end. *Biophys. J.* 91, 2564–2572. doi: 10.1529/biophysj.106.087775.

Paul, A., and Pollard, T. (2008). The Role of the FH1 Domain and Profilin in Formin-Mediated Actin-Filament Elongation and Nucleation. *Current Biology* 18, 9–19. doi: 10.1016/j.cub.2007.11.062.

Perrin, B. J., Strandjord, D. M., Narayanan, P., Henderson, D. M., Johnson, K. R., and Ervasti, J. M. (2013). β-Actin and Fascin-2 Cooperate to Maintain Stereocilia Length. *J. Neurosci.* 33, 8114–8121. doi: 10.1523/JNEUROSCI.0238-13.2013.

Petersen, J., Nielsen, O., Egel, R., and Hagan, I. M. (1998). FH3, A Domain Found in Formins, Targets the Fission Yeast Formin Fus1 to the Projection Tip During Conjugation. *Journal of Cell Biology* 141, 1217–1228. doi: 10.1083/jcb.141.5.1217.

Pfender, S., Kuznetsov, V., Pleiser, S., Kerkhoff, E., and Schuh, M. (2011). Spire-Type Actin Nucleators Cooperate with Formin-2 to Drive Asymmetric Oocyte Division. *Curr Biol* 21, 955–960. doi: 10.1016/j.cub.2011.04.029.

Pfisterer, K., Levitt, J., Lawson, C. D., Marsh, R. J., Heddleston, J. M., Wait, E., et al. (2020). FMNL2 regulates dynamics of fascin in filopodia. *J Cell Biol* 219, e201906111. doi: 10.1083/jcb.201906111.

Pollard, T. D. (2016). Actin and Actin-Binding Proteins. *Cold Spring Harb Perspect Biol* 8, a018226. doi: 10.1101/cshperspect.a018226.

Pollard, T. D., and Cooper, J. A. (1984). Quantitative analysis of the effect of Acanthamoeba profilin on actin filament nucleation and elongation. *Biochemistry* 23, 6631–6641. doi: 10.1021/bi00321a054.

Pollard, T. D., and Wu, J.-Q. (2010). Understanding cytokinesis: lessons from fission yeast. *Nat Rev Mol Cell Biol* 11, 149–155. doi: 10.1038/nrm2834.

Popowicz, G. M., Schleicher, M., Noegel, A. A., and Holak, T. A. (2006). Filamins: promiscuous organizers of the cytoskeleton. *Trends in Biochemical Sciences* 31, 411–419. doi: 10.1016/j.tibs.2006.05.006.

Pring, M., Evangelista, M., Boone, C., Yang, C., and Zigmond, S. H. (2003). Mechanism of Formin-Induced Nucleation of Actin Filaments. *Biochemistry* 42, 486–496. doi: 10.1021/bi026520j.

Pruyne, D. (2016). Revisiting the Phylogeny of the Animal Formins: Two New Subtypes, Relationships with Multiple Wing Hairs Proteins, and a Lost Human Formin. *PLoS One* 11, e0164067. doi: 10.1371/journal.pone.0164067.

Pruyne, D., Evangelista, M., Yang, C., Bi, E., Zigmond, S., Bretscher, A., et al. (2002). Role of Formins in Actin Assembly: Nucleation and Barbed-End Association. *Science* 297, 612–615. doi: 10.1126/science.1072309.

Pruyne, D., Gao, L., Bi, E., and Bretscher, A. (2004). Stable and Dynamic Axes of Polarity Use Distinct Formin Isoforms in Budding Yeast. *MBoC* 15, 4971–4989. doi: 10.1091/mbc.e04-04-0296.

Quinlan, M. E., Heuser, J. E., Kerkhoff, E., and Dyche Mullins, R. (2005). Drosophila Spire is an actin nucleation factor. *Nature* 433, 382–388. doi: 10.1038/nature03241.

Razinia, Z., Mäkelä, T., Ylänne, J., and Calderwood, D. A. (2012). Filamins in mechanosensing and signaling. *Annu Rev Biophys* 41, 227–246. doi: 10.1146/annurev-biophys-050511-102252.

Reymann, A.-C., Boujemaa-Paterski, R., Martiel, J.-L., Guérin, C., Cao, W., Chin, H. F., et al. (2012). Actin Network Architecture Can Determine Myosin Motor Activity. *Science* 336, 1310–1314. doi: 10.1126/science.1221708.

Romero, S., Le Clainche, C., Didry, D., Egile, C., Pantaloni, D., and Carlier, M.-F. (2004). Formin Is a Processive Motor that Requires Profilin to Accelerate Actin Assembly and Associated ATP Hydrolysis. *Cell* 119, 419–429. doi: 10.1016/j.cell.2004.09.039.

Rørth, P. (2009). Collective Cell Migration. *Annual Review of Cell and Developmental Biology* 25, 407–429. doi: 10.1146/annurev.cellbio.042308.113231.

Schirenbeck, A., Bretschneider, T., Arasada, R., Schleicher, M., and Faix, J. (2005). The Diaphanous-related formin dDia2 is required for the formation and maintenance of filopodia. *Nat Cell Biol* 7, 619–625. doi: 10.1038/ncb1266.

Schönichen, A., and Geyer, M. (2010). Fifteen formins for an actin filament: a molecular view on the regulation of human formins. *Biochim Biophys Acta* 1803, 152–163. doi: 10.1016/j.bbamcr.2010.01.014.

Schönichen, A., Mannherz, H. G., Behrmann, E., Mazur, A. J., Kühn, S., Silván, U., et al. (2013). FHOD1 is a combined actin filament capping and bundling factor that selectively associates with actin arcs and stress fibers. *Journal of Cell Science* 126, 1891–1901. doi: 10.1242/jcs.126706.

Schulze, N., Graessl, M., Blancke Soares, A., Geyer, M., Dehmelt, L., and Nalbant, P. (2014). FHOD1 regulates stress fiber organization by controlling the dynamics of transverse arcs and dorsal fibers. *J Cell Sci* 127, 1379–1393. doi: 10.1242/jcs.134627.

Scott, B. J., Neidt, E. M., and Kovar, D. R. (2011). The functionally distinct fission yeast formins have specific actin-assembly properties. *MBoC* 22, 3826–3839. doi: 10.1091/mbc.e11-06-0492.

Sedeh, R. S., Fedorov, A. A., Fedorov, E. V., Ono, S., Matsumura, F., Almo, S. C., et al. (2010). Structure, Evolutionary Conservation, and Conformational Dynamics of Homo sapiens Fascin-1, an F-actin Crosslinking Protein. *Journal of Molecular Biology* 400, 589–604. doi: 10.1016/j.jmb.2010.04.043.

Sept, D., and McCammon, J. A. (2001). Thermodynamics and kinetics of actin filament nucleation. *Biophys. J.* 81, 667–674. doi: 10.1016/S0006-3495(01)75731-1.

Sept, D., Xu, J., Pollard, T. D., and McCammon, J. A. (1999). Annealing accounts for the length of actin filaments formed by spontaneous polymerization. *Biophys J* 77, 2911–2919.

Sherer, L. A., and Courtemanche, N. (2022). Cooperative bundling by fascin generates actin structures with architectures that depend on filament length. *Frontiers in Cell and Developmental Biology. Manuscript in Review*.

Sherer, L. A., Zweifel, M. E., and Courtemanche, N. (2018). Dissection of two parallel pathways for formin-mediated actin filament elongation. *Journal of Biological Chemistry* 293, 17917–17928. doi: 10.1074/jbc.RA118.004845.

Silkworth, W. T., Kunes, K. L., Nickel, G. C., Phillips, M. L., Quinlan, M. E., and Vizcarra, C. L. (2018). The neuron-specific formin Delphilin nucleates nonmuscle actin but does not enhance elongation. *Mol Biol Cell* 29, 610–621. doi: 10.1091/mbc.E17-06-0363.

Sirotkin, V., Berro, J., Macmillan, K., Zhao, L., and Pollard, T. D. (2010). Quantitative Analysis of the Mechanism of Endocytic Actin Patch Assembly and Disassembly in Fission Yeast. *MBoC* 21, 2894–2904. doi: 10.1091/mbc.e10-02-0157.

Sjöblom, B., Salmazo, A., and Djinović-Carugo, K. (2008). Alpha-actinin structure and regulation. *Cell Mol Life Sci* 65, 2688–2701. doi: 10.1007/s00018-008-8080-8.

Skau, C. T., Courson, D. S., Bestul, A. J., Winkelman, J. D., Rock, R. S., Sirotkin, V., et al. (2011). Actin Filament Bundling by Fimbrin Is Important for Endocytosis, Cytokinesis, and Polarization in Fission Yeast *. *Journal of Biological Chemistry* 286, 26964–26977. doi: 10.1074/jbc.M111.239004.

Skau, C. T., Neidt, E. M., and Kovar, D. R. (2009). Role of Tropomyosin in Formin-mediated Contractile Ring Assembly in Fission Yeast. *MBoC* 20, 2160–2173. doi: 10.1091/mbc.e08-12-1201.

Spudich, J. A., and Watt, S. (1971). The Regulation of Rabbit Skeletal Muscle Contraction: I. BIOCHEMICAL STUDIES OF THE INTERACTION OF THE TROPOMYOSIN-TROPONIN COMPLEX WITH ACTIN AND THE PROTEOLYTIC FRAGMENTS OF MYOSIN. *Journal of Biological Chemistry* 246, 4866–4871. doi: 10.1016/S0021-9258(18)62016-2.

Stam, S., Freedman, S. L., Banerjee, S., Weirich, K. L., Dinner, A. R., and Gardel, M. L. (2017). Filament rigidity and connectivity tune the deformation modes of active biopolymer networks. *Proceedings of the National Academy of Sciences* 114, E10037–E10045. doi: 10.1073/pnas.1708625114.

Suzuki, E. L., Chikireddy, J., Dmitrieff, S., Guichard, B., Romet-Lemonne, G., and Jégou, A. (2020). Geometrical Constraints Greatly Hinder Formin mDia1 Activity. *Nano Lett.* 20, 22–32. doi: 10.1021/acs.nanolett.9b02241.

Svitkina, T. (2018). The Actin Cytoskeleton and Actin-Based Motility. *Cold Spring Harb Perspect Biol* 10, a018267. doi: 10.1101/cshperspect.a018267.

Svitkina, T. M. (2020). Actin Cell Cortex: Structure and Molecular Organization. *Trends in Cell Biology* 30, 556–565. doi: 10.1016/j.tcb.2020.03.005.

Tan, V. Y., Lewis, S. J., Adams, J. C., and Martin, R. M. (2013). Association of fascin-1 with mortality, disease progression and metastasis in carcinomas: a systematic review and meta-analysis. *BMC Medicine* 11, 52. doi: 10.1186/1741-7015-11-52.

Tang, H., Bidone, T. C., and Vavylonis, D. (2015). Computational model of polarized actin cables and cytokinetic actin ring formation in budding yeast. *Cytoskeleton (Hoboken)* 72, 517–533. doi: 10.1002/cm.21258.

Thompson, M. E., Heimsath, E. G., Gauvin, T. J., Higgs, H. N., and Kull, F. J. (2013). FMNL3 FH2-actin structure gives insight into formin-mediated actin nucleation and elongation. *Nat Struct Mol Biol* 20, 111–118. doi: 10.1038/nsmb.2462.

Valencia, F. R., Sandoval, E., Du, J., Iu, E., Liu, J., and Plotnikov, S. V. (2021). Force-dependent activation of actin elongation factor mDia1 protects the cytoskeleton from mechanical damage and promotes stress fiber repair. *Dev Cell* 56, 3288-3302.e5. doi: 10.1016/j.devcel.2021.11.004.

Van Audenhove, I., Boucherie, C., Pieters, L., Zwaenepoel, O., Vanloo, B., Martens, E., et al. (2014). Stratifying fascin and cortactin function in invadopodium formation using inhibitory nanobodies and targeted subcellular delocalization. *FASEB J* 28, 1805–1818. doi: 10.1096/fj.13-242537.

Van Audenhove, I., Debeuf, N., Boucherie, C., and Gettemans, J. (2015). Fascin actin bundling controls podosome turnover and disassembly while cortactin is involved in podosome assembly by its SH3 domain in THP-1 macrophages and dendritic cells. *Biochim Biophys Acta* 1853, 940–952. doi: 10.1016/j.bbamcr.2015.01.003.

Van Audenhove, I., Denert, M., Boucherie, C., Pieters, L., Cornelissen, M., and Gettemans, J. (2016). Fascin Rigidity and L-plastin Flexibility Cooperate in Cancer Cell Invadopodia and Filopodia. *J Biol Chem* 291, 9148–9160. doi: 10.1074/jbc.M115.706937.

Vavylonis, D., Kovar, D. R., O'Shaughnessy, B., and Pollard, T. D. (2006). Model of Formin-Associated Actin Filament Elongation. *Molecular Cell* 21, 455–466. doi: 10.1016/j.molcel.2006.01.016.

Vavylonis, D., Wu, J.-Q., Hao, S., O'Shaughnessy, B., and Pollard, T. D. (2008). Assembly Mechanism of the Contractile Ring for Cytokinesis by Fission Yeast. *Science* 319, 97–100. doi: 10.1126/science.1151086.

Vignjevic, D., Kojima, S., Aratyn, Y., Danciu, O., Svitkina, T., and Borisy, G. G. (2006). Role of fascin in filopodial protrusion. *Journal of Cell Biology* 174, 863–875. doi: 10.1083/jcb.200603013.

Watanabe, S., De Zan, T., Ishizaki, T., Yasuda, S., Kamijo, H., Yamada, D., et al. (2013). Loss of a Rho-Regulated Actin Nucleator, mDia2, Impairs Cytokinesis during Mouse Fetal Erythropoiesis. *Cell Reports* 5, 926–932. doi: 10.1016/j.celrep.2013.10.021.

Weaver, A. M. (2006). Invadopodia: specialized cell structures for cancer invasion. *Clin Exp Metastasis* 23, 97–105. doi: 10.1007/s10585-006-9014-1.

Winkelman, J. D., Bilancia, C. G., Peifer, M., and Kovar, D. R. (2014). Ena/VASP Enabled is a highly processive actin polymerase tailored to self-assemble parallel-bundled F-actin networks with Fascin. *Proceedings of the National Academy of Sciences* 111, 4121–4126. doi: 10.1073/pnas.1322093111.

Winkelman, J. D., Suarez, C., Hocky, G. M., Harker, A. J., Morganthaler, A. N., Christensen, J. R., et al. (2016). Fascin- and α-Actinin-Bundled Networks Contain Intrinsic Structural Features that Drive Protein Sorting. *Current Biology* 26, 2697–2706. doi: 10.1016/j.cub.2016.07.080.

Xu, Y., Moseley, J. B., Sagot, I., Poy, F., Pellman, D., Goode, B. L., et al. (2004). Crystal structures of a Formin Homology-2 domain reveal a tethered dimer architecture. *Cell* 116, 711–723. doi: 10.1016/s0092-8674(04)00210-7.

Yamaguchi, H., Ito, Y., Miura, N., Nagamura, Y., Nakabo, A., Fukami, K., et al. (2017). Actinin-1 and actinin-4 play essential but distinct roles in invadopodia formation by carcinoma cells. *European Journal of Cell Biology* 96, 685–694. doi: 10.1016/j.ejcb.2017.07.005.

Yamakita, Y., Matsumura, F., Lipscomb, M. W., Chou, P., Werlen, G., Burkhardt, J. K., et al. (2011). Fascin1 Promotes Cell Migration of Mature Dendritic Cells. *J Immunol* 186, 2850–2859. doi: 10.4049/jimmunol.1001667.

Yamashiro-Matsumura, S., and Matsumura, F. (1985). Purification and characterization of an F-actin-bundling 55-kilodalton protein from HeLa cells. *Journal of Biological Chemistry* 260, 5087–5097. doi: 10.1016/S0021-9258(18)89183-9.

Yamashita, M., Higashi, T., Suetsugu, S., Sato, Y., Ikeda, T., Shirakawa, R., et al. (2007). Crystal structure of human DAAM1 formin homology 2 domain. *Genes to Cells* 12, 1255–1265. doi: 10.1111/j.1365-2443.2007.01132.x.

Yang, C., Czech, L., Gerboth, S., Kojima, S., Scita, G., and Svitkina, T. (2007). Novel Roles of Formin mDia2 in Lamellipodia and Filopodia Formation in Motile Cells. *PLOS Biology* 5, e317. doi: 10.1371/journal.pbio.0050317.

Yang, S., Huang, F.-K., Huang, J., Chen, S., Jakoncic, J., Leo-Macias, A., et al. (2013). Molecular Mechanism of Fascin Function in Filopodial Formation *. *Journal of Biological Chemistry* 288, 274–284. doi: 10.1074/jbc.M112.427971.

Young, M. E., Cooper, J. A., and Bridgman, P. C. (2004). Yeast actin patches are networks of branched actin filaments. *Journal of Cell Biology* 166, 629–635. doi: 10.1083/jcb.200404159.

Zhang, F.-R., Tao, L.-H., Shen, Z.-Y., Lv, Z., Xu, L.-Y., and Li, E.-M. (2008). Fascin Expression in Human Embryonic, Fetal, and Normal Adult Tissue. *J Histochem Cytochem* 56, 193–199. doi: 10.1369/jhc.7A7353.2007.

Zigmond, S. H., Evangelista, M., Boone, C., Yang, C., Dar, A. C., Sicheri, F., et al. (2003). Formin Leaky Cap Allows Elongation in the Presence of Tight Capping Proteins. *Current Biology* 13, 1820–1823. doi: 10.1016/j.cub.2003.09.057.

Zweifel, M. E., and Courtemanche, N. (2020). Competition for delivery of profilin–actin to barbed ends limits the rate of formin-mediated actin filament elongation. *Journal of Biological Chemistry* 295, 4513–4525. doi: 10.1074/jbc.RA119.012000.

Zweifel, M. E., Sherer, L. A., Mahanta, B., and Courtemanche, N. (2021). Nucleation limits the lengths of actin filaments assembled by formin. *Biophysical Journal* 120, 4442–4456. doi: 10.1016/j.bpj.2021.09.003.